JOURNAL OF THERMAL ANALYSIS AND CALORIMETRY 1-12 (2013)

doi:10.1007/s10973-013-2983-9

Solid state thermal degradation behaviour of 1-D coordination polymers of Ni(II) and Cu(II) bridged by conjugated ligand

***Ram Lakhan Prasad*[*1], *Anita Kushwaha*[1], *Imre Miklós Szilágyi*[2] *and László Kótai*[3]**

[1] Department of Chemistry, Faculty of Science, Banaras Hindu University, Varanasi-221005, India.
[2]Research Group of Technical Analytical Chemistry of the Hungarian Academy of Sciences, Department of Inorganic and Analytical Chemistry, Budapest University of Technology and Economics, H–1111 Budapest, Szt. Gellért tér 4. Hungary.
[3] Research Centre for Natural Sciences, Hungarian Academy of Sciences, Pusztaszeri u. 59-67, Budapest, Hungary, H-1025.

Abstract Monometallic complexes $[Cudadb{\cdot}yH_2O]_n$ (**2**) and $[Nidadb{\cdot}yH_2O]_n$ (**3**) and heterobimetallic complex $[Cu_{0.5}Ni_{0.5}dadb.yH_2O]_n$ (**4**) {where $dadbH_2$ = 2,5-Diamino-3,6-dichloro-1,4-benzoquinone (**1**); y = 2-4; n = degree of polymerization} were characterized by elemental analysis, atomic absorption spectroscopy (AAS), infrared spectroscopy (FTIR), powder X-ray diffraction (XRD). The thermal behavior of the complexes was studied by thermal analysis (TG/DTA) under air as well as under helium atmospheres. The released gaseous products were investigated by evolved gas analysis (EGA), performed by an online coupled mass spectrometer (TG/DTA-MS). Thermal degradation of **2** under helium atmosphere is distributed over five steps whereas **3** and **4** exhibited only four degradation steps due to overlap of 2nd and 3rd degradation steps of into one major step. All the complexes exhibit three steps degradation under air. The complex **2** loses NH group in second and HCl/Cl_2, CO groups simultaneously in third steps of decomposition under helium whereas it loses NH and CO groups simultaneously in low temperature region of second step of degradation under air atmosphere as the loss of CO group is facilitated by air. EGA-MS under air and helium atmospheres shows that HCl, CO/CO_2 and $(CN)_2$ fragments are lost simultaneously at multiple steps, and not successively as predicted earlier. Rate of evolution of most evolved gases exhibits several maxima as a consequence of degradation followed by recombination reactions. Final residues under air and helium atmospheres correspond to the metal oxides and metals along with some carbonaceous matter, respectively.

Key words: 1-D coordination polymer, Metal complex, 2,5-Diamino-3,6-dichloro-1,4-benzoquinone, TG/DTA, EGA-MS

*[a] Address for correspondence: Department of Chemistry, Faculty of Science, BHU, Varanasi-221005, India.
Phone: +91-542-6702487, Fax: +91-542-2368127, e-mail: rlpjc@yahoo.co.in

Introduction

Thin film deposition (MOCVD) of metal and metal oxides has been achieved by pyrolytic cleavage of metal complexes for their application in electronic industries [1]. Metal / metal oxides formed under different MOCVD environment exhibit different characteristics, and they have been found to be useful as gas sensors [2], optical switches [3], magnetic storage media [4], lithium batteries [5], and solar cells [6]; owing to their photoconductive, and photochemical and catalytic properties [7].

Thermal degradation pattern of the ligand 2,5-diamino-3,6-dichloro-1,4-benzoquinone (dadb) moiety around Zn(II) ion was found to be different than that around Cu(II) ion [8,9]. Thus coordinated metal ions change the properties of ligand by forming σ and π bonds. The ligand dadb possess conjugation along the molecule [10]. In heterobimetallic complexes two different metal ions are coordinated to the same ligand simultaneously, therefore, there is a possibility of electronic communication between the two metal ions like that of Creutz – Taube ion [11]. Due to electronic communication between the two metal centers in heterobimetallic complexes, the thermal degradation pattern of ligand moieties could be altered / influenced to a significant extent w.r.t their monometallic complexes. With a change in thermal degradation pattern; the morphology, texture, composition and other properties of the useful pyrolytic products might change, and this could be exploited in the above mentioned applications [12]. Therefore, the detailed analysis of thermal decomposition patterns of the metal complexes of dadb is vital for their application in MOCVD and / or other areas.

In view of above, a study of the thermal degradation of metal complexes of dadb with Ni(II) and Cu(II) and their heterobimetallic complexes was undertaken. To the best of our knowledge, no reports are available on thermal degradation of Ni(II) or Cu(II) complexes of dadb, except for a study on thermo-volumetric measurement of cobalt(II), iron(II) and manganese(II) complexes [8] up to 300 °C under nitrogen atmosphere and for one investigation by us on Cu,Zn-dadb complexes [9]. In both previous studies the thermal analysis data were interpreted on the basis of magnitude of mass loss without any evolved gas analysis. Hence, in

the present communication, we are discussing the thermal degradation behaviour of 1-D coordination polymers of Ni(II) and Cu(II) bridged by conjugated ligand. In order to investigate the thermal decomposition of the complexes in detail, the thermal curves were recorded parallelly at different thermal devices (TA Instruments SDT 2920 and Perkin Elmer model Diamond thermal analyzers), at different atmospheres (air and He) and at different heating rates (10 °C/min and 15 °C /min).

Experimental

Materials and methods

Analytical reagent grade chemicals were used. Solvents were purified and dried by standard methods [13] prior to use. The ligand 2,5-diamino-3,6-dichloro-1,4-benzoquinone (dadb) (**1**) was prepared by a previously reported method [8,14,15]. Metal complexes **2, 3** and **4** were synthesized as described elsewhere [9, 16].

Analytical data of the metal complexes

Complex Cu(dadb)·2H_2O **(2):** Colour, blackish green solid; Yield, 65 %; mp >280 °C; Analysis: C, 24.24 ; H, 1.97; N, 8.63%; Calc for Cu($C_6H_2O_2N_2Cl_2$)·2H_2O (M = 304.54): C, 23.65; H, 1.97; N, 9.19%.

Complex **(**Nidadb)·2H_2O (**3),** Colour**,** dark black solid. Yield: 72 %; Decomposition temperature, 268 – 270 °C; Analysis: C, 24.99; H, 2.45; N, 7.88%; Calc. for Ni($C_6H_2O_2N_2Cl_2$)·2H_2O (M = 299.7): C, 24.02; H, 2.00; N, 9.34%,.

Complex $Cu_{0.5}Ni_{0.5}$(dadb)·2H_2O (**4**): Colour, dark green solid; Yield, 77 %; temperature, 278 – 280 ºC. Analysis: Ni, 9.10; Cu, 10.17; C, 22.95; H, 1.52; N, 9.98%; Calc. for $Cu_{0.5}Ni_{0.5}$($C_6H_2O_2N_2Cl_2$)·2H_2O (M = 302.12) : Ni, 9.71; Cu, 10.52; C, 23.83; H, 1.98; N, 9.27%.

Instrumentation

Elemental analysis (carbon, hydrogen and nitrogen) were performed on an Elemental Analyzer model Carlo Erba 1108. Copper and nickel metal analysis were performed by atomic absorption spectrophotometer (AAS) using Perkin Elmer AAnalyst-300 Spectrometer. The melting points of the complexes were determined in open capillaries using Gallenkamp apparatus and are uncorrected. IR spectra (KBR disc) were recorded on a VARIAN 3100 FT-IR

spectrophotometer in the region 4000 - 400 cm^{-1}. The X–ray powder diffraction (PXRD) patterns of **3** and **4** were recorded on a Rigaku D/Max–B powder X–ray diffractometer with Cu Kα radiation. PXRD of **2** was recorded on a SEIFERT X–ray diffractometer using Cu Kα radiation. Thermal analytical (TG/DTA) were recorded on the one hand on a Perkin Elmer model Diamond (PED) TG/DTA thermal analyzer using alumina crucible at the heating rate 15 °C/ min in air. DSC curves were measured on a Mettler Toledo TC 15 TA differential scanning calorimeter at 5 °C min^{-1} under nitrogen atmosphere using pure grade indium as standard by taking samples in closed lid aluminum pan in temperature range RT – 300 °C. During the evolved gas analytical (TG/DTA-MS) measurements, an open platinum crucible, sample sizes of 7-20 mg, and heating rates of 10 and 15 °C min^{-1} were used. The thermoanalytical furnace was purged with air or He with a flowing rate of 130 ml min^{-1}. The TG/DTA-MS apparatus consisted of an STD 2960 Simultaneous DTA/TG (TA Instruments Inc.) thermal analyzer and a Thermostar GSD 200 (Balzers Instruments) quadrupole mass spectrometer. On-line coupling between the two parts was provided through a heated (T = 200 °C) 100 % methyl deactivated fused silica capillary tube with inner diameter of 0.15 mm. Selected ions between m/z = 1-133 were monitored through 33 channels in Multiple Ion Detection Mode (MID) with a measuring time of 0.5 s per channel.

Results and discussion

Results of experimental C, H, N and metal analyses for the complexes match with the calculated values. The solid complexes are stable in presence of air but weakly hygroscopic. Complexes dried over $CaCl_2$ under vacuo gain some mass on exposure to air and extent of mass gain depends upon relative humidity present in the air. Complexes decompose in the temperature range 270 – 280 ^oC. All the metal complexes are insoluble in common organic solvents such as ethanol, methanol, acetone, chloroform, dichloromethane, ether and benzene as well as highly polar solvents like DMF and DMSO.

IR spectra

The IR spectrum of the ligand dadb exhibits two bands at 3308 and 3376 cm^{-1} due to $\nu_s(NH_2)_{opc}$ and $\nu_{as}(NH_2)_{opc}$ modes of the NH_2 groups, while other characteristic bands of the ligand at 1667, 1616 and 1580 cm^{-1} (Table S1) are assigned to ν(C=O), ν(C=C ring) and βNH_2 modes of vibrations, respectively [10]. A new band appearing in the range 3404 – 3470 cm^{-1} in

the metal complexes is assigned to ν(OH) stretching frequencies which are absent in the free ligand. Appearance of absorption band due to ν(OH) stretching frequencies indicates the presence of water molecules in the metal complexes of dadb. The IR spectra of the metal complexes show a single band in the region of 3280 – 3340 cm^{-1} due to ν_{as}(N – H) stretching vibration. Presence of single ν_{as}(N–H) stretching vibration in the metal complexes indicates that one of the hydrogen atoms of NH_2 groups is absent due to deprotonation. The decrease of the wavenumber value for the NH stretching vibration of the metal complexes as compared to that of the free ligand dadb suggests that nitrogen atom of the NH group is involved in coordination [17]. In metal complexes of dadb the asymmetric (C=O) stretching vibrational mode is observed in the range 1610 – 1655 cm^{-1} either as medium intensity shoulder or distinct peak. Thus lowering of ν(C=O) frequency in the metal complexes is in favour of coordinated nature of carbonyl group [18] of the ligand. The ν(C=C) and βNH_2 vibration modes of the ligand merge and yield a single broad band in the metal complexes except for **2** where ν(C= C) is observed as distinct shoulder at 1542 cm^{-1} and βNH_2 mode as very strong peak at 1494 cm^{-1}. Shifting of these bands to lower wavenumbers in the metal complexes as compared to that of the free ligand dadb value supports coordination through nitrogen and oxygen atoms of the ligand in monometallic as well as in heterobimetallic complexes [8, 17, 18].

Powder X-ray diffraction (PXRD)

Ligand **1** exhibits two intense lines at 2θ values ~ 31.6° and 45.4° in its powder X-ray diffraction (PXRD) spectrum which are absent in their metal complexes. PXRD patterns of the complexes **2 – 4** recorded between 2θ values 20° to 80° exhibit many lines, which are however broader than that of **1.** Presence of several lines in PXRD of complexes suggests the crystalline [19-21] nature of them. Here we restrict the discussion to more intense peaks only. The first intense peak at ~ 21.5° is relatively weak in monometallic complexes **2** and **3** as compared to that present in heterobimetallic complex **4,** however it is found at an almost similar position (Table S2, Fig. 1). The second peak is more intense and sharper and is observed at 2θ values ~ 22.34° and 22.48° in diffractogram of **2** and **3**, respectively. Position of this peak is shifted towards higher 2θ values (with ~ 0.5°) in heterobimetallic complex **4**. Further, separation between first and second intense peaks of heterobimetallic complex **4** (1.62°) is much larger than at monometallic complexes **2** (0.65°) and **3** (1.06°). The more intense peaks observed at 2θ values

27.08°, 27.68° and 27.85° at **4** merged into one peak in monometallic complex **2** whereas they are observed as single peak at 26.72° in **3.** Third peak is shifted to toward higher 2θ values in heterobimetallic complexes **4** (28.18°) and its intensity is much higher than those of the monometallic complexes **2** and **3**. There are no intense peaks in PXRD of monometallic complex **3** in the range of 2θ values 30 – 37°, however, two weak peaks at 2θ values 33.08° and 34.32° are visible in the diffractogram of **2**. Heterobimetallic complex **4** also exhibits two peaks at 32.59 and 34.37° in above region whose intensities are higher and peaks are much sharper than at **2**. Further, former peak is shifted to lower 2θ value and latter peak is observed at almost similar position as at **2**. Thus, in going from monometallic to heterobimetallic complexes positions of some of the PXRD peak of monometallic complexes remains unchanged whereas other are shifted and their intensities changes. These features indicate that heterobimetallic complex **4** may not be mixture of monometallic complexes **2** and **3**, consequently, it is concluded that heterobimetallic complex **4** exhibits a distinctly new species.

Thermal analysis

Simultaneously recorded TG/DTA curves of the complexes **2**, **3** and **4** on the TA Instruments device with heating rate 10 under air and 15 °C/min under helium atmospheres along with EGA-MS scan of evolved fragments from **2** with selected m/z values are presented Figure 2 and 3, respectively. TG/DTA curves of **2, 3** and **4** with heating rate 15 °C/min and simultaneous EGA -MS curves of **2**, **3**, and **4** with heating rates 15 °C/min under air atmosphere are presented in Figures S1 and S2a-c respectively. EGA-MS curves of the complexes **2, 3** and **4** with heating rate 15 °C/min under helium and air atmospheres are presented in figures S3 and S4, respectively. The data of magnitude of mass losses, DTG, DTA peak positions, and evolved gases, in particular temperature ranges of all the complexes are collected in Table S3 a-e. TG/DTA of the complexes **2**, **3** and **4** were also recorded on Perkin Elmer model Diamond (PED) thermal analyzer under air atmosphere and pertinent data are included in Table S3a-c and Figure 4. TG/DTA-MS data recorded on the TA Instruments device particularly at heating rate 10 °C /min in air and 15 °C /min in helium atmospheres are being discussed in detail followed by correlation of the data with each other and data recorded on PED thermal analyzer.

Loss of water molecules from the complexes

First stage of mass loss corresponds to the loss of water molecules under air as well as helium atmospheres for all the complexes. Water molecules in the complex **2** exist as crystalline /adsorbed water [9]. Existence of two distinct endothermic peaks at ~ 64 and 187 °C in DSC curve of **3** corresponding to surface / crystalline water indicates that water molecules are coordinated to metal ions in the complex **3**. Presence of signals at m/z 19 $(H_3O)^+$, 18 (H_2O) and 17 (OH) in EGA-MS spectra (Fig. 2, Fig. 3 and Fig. S2, S3, S4) confirms the loss of water molecules from all the complexes under first step of thermal degradation.

*Thermal behaviour of **2** with heating rate 10 °C /min under air atmosphere*

After loss of water molecules in first step of degradation, the anhydrous complexes are obtained. Actual degradation of ligand fragments from anhydrous complexes takes place at 2nd and 3rd step of thermal degradation. TG curve of **2** indicates that 2nd step of thermal degradation loses ~ 57.25 % of mass in the temperature range 200 – 325 °C under air atmosphere (Table S3a, Fig. 2). This step of thermal degradation exhibits two exothermic DTA peaks (250 and 311 °C). The DTA peaks at lower (~246 °C) and higher temperatures (~310 °C) are consistent with maxima observed in the simultaneous EGA-MS scan for the rate of evolved gases with m/z value corresponding to H_2O, NH_3/OH, NO, NO_2, CO_2 at ~ 247 °C and NO, NO_2, CO_2, $(CN)_2$, HCl, Cl_2, and some ligand fragments at ~ 310 °C, respectively. This indicates that CO and NH groups of ligand are degrading at lower temperature and HCl / Cl_2 at higher temperature during second step of thermal degradation. Previous reports studied the formation of gaseous product H_2O, NO and N_2O on combustion of ligand fragments NH_3/NH_2/NH [22-23]. However, we have observed that the ligand fragment NH yields an additional combustion product NO_2 (m/z 46) in addition to the previously reported fragments in same temperature regions (Fig. 2, Fig. S2a). HCl gives two signals at m/z 36 and 38 and Cl_2 exhibits two signals m/z 70 and 72 due to isotope distribution of chlorine atom 35 and 37, respectively (Fig. S2a). The m/z signal corresponding to HCl are stronger than that of Cl_2, therefore, it appears that HCl is actually being lost from ligand and it is oxidized into Cl_2 and H_2O under air atmosphere or HCl molecule undergoes dissociation and recombination to produce Cl_2 as daughter molecules under the condition of mass spectrometer. Carbonyl group is oxidized to CO_2, therefore, signal corresponding CO (28) is absent from the MS scan and that of CO_2 are being prominently observed. After 2nd step of degradation and before onset of 3rd step of thermal degradation there is slight mass gain (0.5 %) rather than mass

loss in the temperature range 325 – 430 °C, however, EGA-MS scan under this temperature range shows the loss of trace amount of HCl, Cl_2, CO_2, and $(CN)_2$. Thus, net mass gain in spite of slight mass losses indicates that there is some uptake of oxygen by complex residue. At 3rd step of degradation a mass loss of 10.25 % is observed in temperature range 430 – 600 °C. The EGA-MS scan under this step shows that $(CN)_2$, HCl, Cl_2, traces of CO_2 and some ligand fragment are lost under this step. The residue obtained at end of this step (26 %) is slightly less than that expected for one mole of CuO (calc. 27.4 %), however the residue gains some mass in temperature range 600 – 900 °C and final residue (27.6 %) at ~ 900 °C is found to be consistent with calculated value for one mole of CuO [9,24-26]. Thus, thermal degradation of **2** under air atmosphere essentially takes place in three steps.

*Thermal behaviour of **2** with heating rate 15 °C /min under air atmosphere*

On increasing the heating rate from 10 °C/min to 15 °C/min the 2nd step of thermal degradation in the temperature range 200 – 322 °C split into visibly three distinct regions from 200 – 257, 257 – 310 and 310 –304 – 337 °C (Table 2 a, Fig. S1 and S 4a). In the temperature ranges 200 – 257 and 257 – 310 °C the DTA peaks are found to be at almost same position as in the curves with heating rate 10 °C/min. However, in the TG curve with heating rate 15 °C/min the two regions are distinguishable whereas in TG curve with heating rate 10 °C/min is not. EGA-MS scan indicates the evolution of same fragments in above temperature regions on both heating rates of the complex **2** (Fig. S2a and Fig. S 4a). In the temperature range 310 – 337 °C, a new DTA peak is observed ~ 325 °C which was absent from the curves with heating rate 10 °C/min. EGA-MS curve shows the evolution of same fragments in temperature region 310 – 337 °C as in 257 – 310 °C. Thus, in the EGA-MS curve the three distinct maxima/ peaks for the rate of evolution of fragments are observed at ~ 252, 283 and 324 °C in the temperature ranges 200 – 257, 257 – 310 and 310 –304 – 337 °C, respectively (Fig. S4a). However, the complex **2** with heating rate 10 °C/min exhibits only two maxima in this temperature range. Further, summation of the mass losses in three split sub-steps from the curve of **2** with heating rate 15 °C/min is close to that of 2nd step of thermal degradation with heating rate 10 °C/min. The TG curve of **2** with heating rate 15 °C/min beyond 2nd step of thermal degradation is almost the same as in case of TG curve with heating rate 10 °C/min, however, final residue from the curve with heating rate 15 °C/min is less than that of the heating rate 10 °C/min.

*Comparison of thermal curves of **2** recorded on TA and PED devices under air atmosphere*

TG curves of **2** with heating rate 15 °C/min recorded on PED thermal analyzer also exhibits split of 2nd step of thermal degradation into three regions but spanned over slightly higher temperature ranges 200 – 297, 297-284-330 and 330 – 420 °C like that recorded on the TA Instr. device (Fig. 4 and Fig. S1). The summation of mass losses under these three steps from TG curve recorded on PED thermal analyzer were found to be same as in case of curve on TA instrument with same heating rate (Table S3 a). TG curves recorded on TA and PED thermal analyzer with same heating rate (15 °C/ min) exhibit non ideal nature of the curves in the temperature regions 310 – 304 – 337 and 297 – 284 – 297 °C, respectively. There is a sudden decrease of temperature between these regions. The time-temperature profiles seem to be affected by the exothermic character of the processes in this region to yield non ideal curves. Curves recorded at both instruments are qualitatively similar though the non ideal character is less marked on the curves of TA Instr. device than that of PE device. However, the non-ideal nature of the curves on slower heating rate (10°C /min) reduces to such an extent that resultant curve appears as normal at glance (Fig. 2). Thus curves recorded at PED and TA Instr. thermal analyzer are almost similar but not identical. It would be worth to be mentioned that in absence of EGA it was speculated that HCl, CO and $(CN)_2$ fragments are lost from **2** on thermal degradation successively with increasing temperature purely on the basis of magnitude of mass losses at different steps [9]. However, on the EGA-MS analysis of **2** under air in the present study shows that HCl, CO/CO_2 and $(CN)_2$ fragments are being lost simultaneously at multiple steps not successively at different stages as predicted earlier. Final residue from curves recorded on PED thermal analyzer with heating rate 15°C/min and TA Instr. thermal analyzer with heating rate 10 °C/min correspond to one mole of CuO [9]. In a previous communication, we characterized the final residue by comparing powder XRD of residue of **2** and freshly prepared CuO [27] followed by matching with JCPDS file of CuO (5–661) to confirm the formation of CuO as residue under air atmosphere. However, curves recorded on TA Instr. thermal analyzer with heating rate 15 °C/min yields much lower residue that that calculated for one mole of CuO. It seems that due to exothermic nature of degradation process some of the residual mass fly away from open platinum crucible during degradation when heating rate is high and consequently yields smaller magnitude of residue for the heating rate 15 °C/min as compared to that of the heating rate 10 °C/min.

*Thermal behaviour of **3** and **4** under air atmosphere recorded at different heating rates and different devices.*

Thermal degradation of **3** and **4** under air atmosphere with heating rate 10 °C/min also takes place in three stages (Table S3 b – c and Fig. 2,) similar to that of **2** except absence of plateau between 2nd and 3rd stage of degradation in temperature range 330 – 420 °C. On the basis of onset of thermal degradation for 2nd step of degradation, the thermal stability of the complexes can be arranged in order; **3** > **4** > **2**. Further, almost similar fragments are lost from **3** and **4** under air atmosphere as in case of **2** (Fig. S 3b-c). Magnitude of final residue on pyrolysis of **3** and **4** matches with one mole of NiO [28] and $Cu_{0.5}Ni_{0.5}O$, respectively. TG curves of **3** and **4** with heating rate 15 °C/min was found to be super imposable on the respective TG curve recorded at heating rate 10 °C/min except final residue is found to be less than that expected for one mole of metal oxide of the metal present in the respective complexes as in case of **2 (**Fig. S 5 b-c**)**. TG curve of **3** recorded on PED thermal analyzer exhibits non ideal curve in the temperature range 398 – 394 – 400 °C as in case of **2**, however, the magnitude of final residue is higher than that expected for one mole of NiO and it is not constant even up to 900 °C (Fig. 4 and Fig. S 5b). TG curve of **4** recorded on PED thermal analyzer also exhibits three step of degradation like that on TA Instr. device with heating rate 10 °C/min. Further, TG curve of **4** recorded at PED shows that the onset of thermal degradation of ligand moiety (2nd step of degradation) takes place at lower temperature than that recorded on TA i Instr. device but final residue was consistent with one mole of metal oxide of the metals present in the complex **4** as in the case of the TG curve with heating rate 10 °C / min recorded on TA Instr. device. Thus, thermal curves recorded on different thermal analyzers are qualitatively similar. Final residue obtained from TG curve of **4** with heating rate 15 °C/min recorded on TA Instr. device was found to be lower than that calculated for metal oxides, and lower than those of other complexes under same condition.

*Conclusions drawn from thermal behaviour of **2, 3** and **4** under air atmosphere*

Onset of thermal degradation of anhydrous complex **2** (2nd step of degradation) at lower temperature than that of **3** indicates that degradation of the ligand moiety is significantly influenced / accelerated by copper(II) ions bonded to it as compared to that of nickel(II) ions. Therefore, all the ligand dadb moiety directly bonded with copper(II) metal ions in the heterobimetallic complex **4**, would be expected to start degrading at almost same temperature as

in case of **2**. Contrary to above, the onset of 2nd stage of degradation of **4** takes place at intermediate temperature between those of **2** and **3**, probably due to change of electronic environment on Cu(II) atoms of **4** as a consequence of electronic communication between Cu(II) and Ni(II) ions bridged by π-conjugated dadb ligand [10,16]. Onset of degradation of **4** at higher temperature than that of **2** indicates that the ligand dadb moiety is less destabilized in **4** as compared to that of **2.** Thus thermal degradation pattern of the complex **4** indirectly corroborates the finding of electronic communication between two metal ions bridged by π-conjugated ligand [16]. Similar correlation is found with DTA data given in Table S3a-c and Fig. 2 for the complexes **2**, **3** and **4**.

Identical ion fragments are evolved in almost identical sequence from **2**, **3** and **4** during thermal degradation under air atmosphere at the heating rate 10 °C/min, however they are evolved at different temperature regions. Fig. 6 shows that a same set of ions derived from fragments H_2O, NH, and CO (m/z 18, 52 and 44) are evolved from **2, 3** and **4** around 250, ~340 and ~ 290 °C, respectively. Second set of ions corresponding to CO_2, HCl and $(CN)_2$ are evolved from **2**, **3** and **4** with maxima for the rate of evolution at the temperatures ~ 310, 370 and 326 °C, respectively. Thus, same set of evolved gases are released from the heterobimetallic complex **4** at intermediate temperature between those for the monometallic complexes **2** and **3**. Second maxima for the rate of loss of HCl and $(CN)_2$ are found at the temperatures 560, 580 and ~ 500 °C from **2, 3** and **4**, respectively. Further, the second maxima for the loss of CO_2 from **3** is found to be at 560 °C as strong peak and from **2** at 450, 500 and 690 °C with relatively smaller signals, however, in case of **4,** the corresponding signal is found at much lower temperature (450 °C) but as strong peak. This indicate that the second signals at higher temperature for the loss of HCl, $(CN)_2$ and CO_2 are being observed at much lower temperature from the heterobimetallic complex **4** than those of monometallic complexes **2** and **3**. EGA-MS results show the multiple maxima for the rate of evolution of a particular fragment at different temperatures during thermal degradation of the complexes i.e. fragments are released periodically at different intervals of temperature.

*Thermal behaviour of **2** under helium atmosphere*

After loss of water molecules at first step of degradation, the complex **2** losses ~ 6 % of mass at 2nd stage of thermal degradation of **2** under helium atmosphere in the temperature range

180 – 260 °C (Table S3d, Fig. 3, Fig. S5a). EGA-MS scan for this step of degradation exhibits m/z peaks corresponding to H_2O (19, 18, 17), NH_3/ NH_2/NH (17, 16, 15, 14) recombination/combustion product of NH_3/ NH_2/NH like NO (30), N_2O (44), NO_2 (46), HCN (27), $(CN)_2$ (52, 26), and small amount of other ligand fragments (Fig. 3 and Fig. S3a). This indicates that mainly NH moiety of ligand is being lost in addition to the loss of remaining water molecules under this step of degradation. Loss of water molecules are almost completed under this step as the MS signal corresponding to m/z 18 and 17 ceases beyond this temperatures range. The DTA curve for this step of degradation reveals that the loss of H_2O, NH group and other ligand fragments from complex **2** is endothermic. Highest magnitude of mass loss (36 %) is observed under third step of thermal degradation (260-480 °C) under helium atmosphere with exothermic DTA peak at 350 °C. EGA-MS signals in this temperature range indicates that the loss of chlorine as HCl /Cl_2 and loss of CO also starts to take place under this step in addition to the loss of fragments as in case of 2nd step. Thus it could be concluded that the exothermic nature of this step is due to release of HCl /Cl_2 and CO molecules as additional fragments released during this step are same as in case of 2nd step of degradation which is endothermic. Rate of loss of all the fragments initially increases and attain maxima ~ 360 °C followed by decrease to minima ~ 480 °C. EGA-MS scan for the fourth step of thermal degradation exhibiting 20 % mass loss under helium atmosphere shows that the rate of evolution of signals corresponding to HCl and Cl_2 increases from 480 to 620 °C followed by gradual decrease whereas signals for NO, HCN, $(CN)_2$ and some ligand fragments acquire maxima ~ 660 °C. TG curve indicates that 4th step is endothermic. EGA-MS scan for the fifth step of thermal degradation exhibiting ~ 3 % mass loss shows the presence of signals corresponding to the traces of CO, HCN, CN in temperature range 760 – 900 °C i.e. 5th step is an offshoot of 4th step of degradation. Final residue ~ 28 % is expected to contain metallic copper [24, 29-31] along with some carbonaceous matter at 900 °C.

*Thermal behaviour of **3** and **4** under helium atmosphere*

Onsets of thermal degradation of anhydrous complexes (second stage of decomposition) under helium atmosphere of **2**, **3** and **4** take place at 170, 320 and 280 °C, respectively. Therefore, the thermal stability of anhydrous complexes under helium atmosphere may be arranged as **3** > **4** > **2**, a similar trend as in case of air atmosphere. Simultaneous EGA-MS scan

for the 2nd step of thermal degradation of **3** exhibits two maxima for the rate of loss of fragments at 356 and 385 °C. The maxima at lower temperature (356 °C) of **3** shows same signals for the evolution of fragments as in case of second step of degradation of **2.** Similarly, a maxima at higher temperature (385 °C) arises due to evolution of almost identical fragments as in case of third step of degradation of **2**. This indicates that 2nd and 3rd step of degradation in **3** are so close to each other that they merge into each other and yield only one curvature in TG curve for this combined step unlike that of **2** (Fig. 3 and Fig. S5 a-b). Complex **4** also exhibits similar thermal behaviour for 2nd and 3rd steps of thermal degradation as in case of **3**. It is interesting to note that thermal degradation of 3rd step of **2** and combined 2nd and 3rd steps of **3** under helium atmosphere take place ~ 340 – 350 °C whereas combined 2nd and 3rd step of degradation of heterobimetallic complex **4** occurs at much lower temperature ~ 300 °C than those of **2** and **3** unlike that under air atmosphere (Fig. 3 and Fig. S6). 4th step of thermal degradation of **3** takes place in the temperature range 440 -700 °C with a maxima for the rate of loss of fragments at 550 °C for the ions characteristic of mainly HCl/ Cl_2 and small amount of CO and another maxima at 630 °C for the ions characteristic of $(CN)_2$ (26) (Fig. S3b). Unlike **3** the complex **4** exhibits only one maxima at the 4th step of thermal degradation for the rate of loss of ions characteristic of mainly HCl/ Cl_2, small amount of CO and other ligand fragments around 580 °C. Only very small amount of CO, and CN are evolved under 5th step of thermal degradation of **3** and **4** similarly as at **2**. 4th and 5th steps of thermal degradation of the complexes **2**, **3** and **4** take place at almost identical temperatures, however, the maxima for rate of evolution of fragments ions for **4** are observed at intermediate temperature between those of **2** and **3** like 2nd step of degradation. It is worth to be mentioned here that last maxima for the evolution of HCl/ Cl_2 from the complex **4** under air atmosphere occurs at lower temperature than those for the monometallic complexes **2** and **3** whereas under helium atmosphere it occurs at intermediate temperature between those of **2** and **3**. TG curves of **2**, **3** and **4** are almost alike except second step of thermal degradation of **3** and **4** are shifted to higher temperature to such an extent that 2nd and 3rd step of degradations are clubbed into one step. Consequently, the TG curves of **3** and **4** appear to exhibit four steps whereas **2** shows five steps of thermal degradation at a glance. Magnitude of final residue from all the three complexes is higher than that calculated for one mole of metal [28, 29-31] probably due to carbonaceous matter alongwith reduced metal. Further, it is worth to be mentioned that re-

recorded TG curve of the heterobimetallic complex **4** on simultaneous TGA/DTA-MS device is superimposable on its original TG curve (Fig. S5b).

Mysterious pattern of thermal degradation of metal complexes of dadb

The losses of NH group and some ligand fragments from **2** under helium atmosphere are endothermic under 2nd step of degradation. Earlier it was concluded that the exothermic nature of 3rd step is due to release of HCl /Cl_2 and CO molecules because additional fragments released during this step are same as in case of 2nd step of degradation which are endothermic. Contrary to the exothermic nature of evolution of HCl /Cl_2 and CO molecules in 3rd step, the evolution of same component under 4th step of thermal degradation is endothermic (Table S3d, Fig. 3, Fig. S3a). This unusual behaviour is mysterious at a glance

Further, simultaneous EGA-MS scan for **2** under helium atmosphere shows that the rate of losses of most of the fragments like HCl / Cl_2, CO and HCN/$(CN)_2$ under 3rd step is accelerated from ~ 280 °C to ~ 350 °C followed by de-acceleration to a minima ~ 480 °C. Subsequently, another maxima (~ 620 °C) for the rate of losses of HCl / Cl_2 and some other ligand fragments is obtained in temperature range 480 - 760 °C. Similarly, the loss of H_2O takes place in the two regions RT-200 and 200 – 260 °C. However the losses of water molecules at higher temperature range may be due recombination reaction between fragment NH group and oxygen atoms to yield the products H_2O and oxides of nitrogen (NO, N_2O and NO_2) as maxima for the rate of losses of oxides of nitrogen as well as water are observed at almost same temperature in EGA-MS scan. Normally one would expect that one component would be lost at a stretch i.e. one maxima is expected in simultaneous EGA-MS curve of the complexes for the loss of a particular component but multiple maxima are observed periodically for the losses of most of the components during thermal degradation under helium as well as under air atmospheres. Periodic release of identical fragments at different temperatures during thermal degradation of the metal complexes with dadb is 2nd mystery.

Factors responsible for mysterious thermal degradation

Pyrolysis of metal complexes might take place in the following way; (i) the metal complexes may lose the fragments successively one by one starting from loosely bound to strongly bound. (ii) degradation of all the fragments might occur at temperatures very close to

each other i.e. practically all the fragments are release simultaneously and degradation of the complexes might proceed from surface to core of the bulk during heating. On the basis of second assumption a particular fragment ion should continuously be lost till the all the complex degrades and only one maxima for rate of evolution for the fragment is expected. Completion of thermal degradation of metal complexes in multiple steps and observation of multiple maxima for the rate of evolution of most of the fragments i.e. periodic losses of fragments in different temperature ranges under air and helium atmospheres indicate that second assumption is ruled out. Simultaneous EGA-MS scan of **2** under helium atmosphere showing the loss of water molecules at first step, NH group at second step and HCl/Cl_2 and CO groups at third step of degradation indicates that first assumption is applicable for the degradation of the complexes under present study.

Appearance of multiple maxima for the rate of evolution of the fragments in EGA-MS curves could be possible in following two conditions (a) when a particular group/atom is attached with ligand at more than one site and the groups/ atoms at each site possess different environment, they would be lost at different temperatures to yield multiple maxima for evolution of same fragment and (b) when a fraction of pyrolysis product recombines with complex residue to form thermally stable product at that temperature range and rest fraction escapes. The recombined product could degrade at higher temperatures and yield second maxima for the loss of fragments and so on. The dadb molecule possesses chemically and electronically equivalent two >C = O, > NH and C – Cl bonds [10], therefore, first condition (a) is not applicable. In view of above, the second condition (b) is the only option left to yield multiple maxima of evolved gas at different temperatures i.e. periodic evolution of CO, NH and HCl/Cl_2. Under such circumstances, the number of maxima for the rate of evolution of particular fragments would depend upon number of cycles of degradation followed by recombination of a fraction of fragments with complex residue containing metal and allowing another fraction to escape at each step. Thus, 2nd mystery of periodic release of identical fragments like CO, $NH/(CN)_2$ and HCl/Cl_2 at different temperatures during thermal degradation of the metal complexes with dadb arises due to degradation of these fragments from the complexes followed by recombination of these fragments with the complex residue.

Third step of thermal degradation with losses of HCl/Cl_2 and CO from **2** under helium atmosphere should also be endothermic as energy is required for breaking of bonds as in the case

of 2nd and 4th steps of degradation. Periodic release of the identical fragments like HCl/Cl_2 and $(CN)_2$ at 3rd and 4th steps of degradation indicates that a fraction of evolved gases HCl/Cl_2 and $(CN)_2$ escapes and other fraction recombines with residue to form a stable complex under 3rd step of degradation. Recombination reaction between a fraction of liberated HCl/Cl_2 and $(CN)_2$ molecules and residual mass generates heat to overcome the heat absorbed during pyrolysis at this step of degradation. Therefore, a net heat is released over third step of degradation. Further, the recombined complex residual mass of third step commences to decompose beyond 480 °C and loses HCl and Cl_2 in 4th step of degradation. Due to absence of recombination reactions between liberated HCl/Cl_2 and $(CN)_2$ molecules and metal residue under 4th step of degradation, no heat is evolved under this step. Consequently, 4th step of degradation is endothermic in spite of same fragments are being released under this step like those under 3rd step of degradation. Thus because of recombination of a fraction of evolved gases with residual mass, the thermal degradation under 3rd step becomes exothermic whereas 4th step of degradation remains endothermic in absence of recombination reactions. Thus first mystery of 3rd step of degradation being exothermic and 4th step endothermic in spite of evolution of same gases under both steps is explained by recombination of a fraction of evolved gases with complex residue of **2** in third step and no reaction between evolved gases and complex residue in 4th step.

Further, EGA-MS scan shows the presence of signals at m/z 30 (NO), 44 (N_2O) and 46 (NO_2) which could arise due to combustion of the fragment NH group from 2nd to 4th step of degradation. Further, the signal at m/z 44 might have some contribution from CO_2 as combustion of CO. Presence of these signals indicates that some traces of oxygen seems to be still remaining in devices in spite of all the precaution. Therefore, all the three steps of degradation (2nd, 3rd and 4th steps) may have some contributions due to above reaction exothermic combustions. It is not possible to quantify the magnitude of exothermic contributions in individual step. However, Presence of significant magnitude of signal characteristic to CO (28) it can be concluded that the presence of oxygen is insignificant. Under these circumstances, the mysterious exothermic nature of 3rd step and endothermic character of 2nd and 4th steps of degradation might be qualitatively correct as per explanation cited above but it could not be conclusive.

Role of air (oxygen) on the thermal degradation of complexes

Second step of thermal degradation of **2** occurs at almost same temperature under air as well as under helium atmospheres (Fig. S5a, Fig. S6), however, 3rd step of thermal degradation under air takes place at lower temperature than that of helium atmosphere. Further, loss of CO group (m/z 28) takes place at 3rd step of degradation under helium atmosphere (Fig. S3a) whereas loss of CO_2 occurs prominently at 2nd step of degradation of **2** under air (Fig. S2a). This indicates that oxygen molecules under air atmosphere attacks the carbonyl group of ligand and helps the breaking of C – C bond attached to carbonyl group and release CO_2. Consequently, CO group is lost from the ligand residue at lower temperature under air than that under helium atmosphere. Thus air accelerates the loss of CO group from ligand residue. Thermal degradation of combined step (2nd and 3rd) of the complexes 3 and 4 occurs at almost same temperature under air as well as helium atmospheres (Fig. S5 b-c, Fig. S6).

Conclusions

Monometallic 1-D coordination polymer of Cu(II) **2** and Ni(II) **3** and heterobimetallic complex using Cu(II) and Ni(II) **4** with conjugated ligand dadb were synthesized by reported method and characterized by elemental analysis, FT-IR, powder X-ray diffraction (XRD) and simultaneous TG/DTA-MS analysis. FT-IR indicated bonding of metals to ligand through nitrogen and oxygen donor atoms of the NH and quinonic carbonyl group, respectively, of the ligand dadb. Powder XRD of the monometallic complexes **2**, **3** and **4** shows several distinct peaks indicating crystalline nature of all the three complexes [16]. Further, powder XRD shows that heterobimetallic complex **4** exhibits distinctly different nature from those of monometallic complexes **2** and **3**.

Evolution of gaseous product has been analyzed and monitored by online coupled TG/DTA-MS spectrometer under air as well as under helium atmospheres. Particularly, the complex **2** exhibits excellent EGA-MS curves of evolved gases under helium atmosphere to reveal the mystery of thermal degradation. The complex **2** lose mainly water and NH group of the ligand moiety under first and second step of thermal degradation, respectively. DTA curve indicates that first and second steps of degradation under helium atmosphere are endothermic probably due to energy requirement to break the bonds. HCl/Cl_2 and CO molecules are mainly lost under 3rd step of thermal degradation in addition to the loss of remaining NH_2, $[HCN]/(CN)_2$, and some ligand fragments, however, this step is exothermic in contrast to endothermic nature of

2nd and 4th steps of degradation of **2** under helium atmosphere. Forth step of degradation also shows the loss of HCl / Cl_2 and CO molecules as major component but this step is mysteriously endothermic contrary to 3rd step of degradation. Further, it has been observed from EGA-MS curves that the rate of loss of NH, HCN/$(CN)_2$, CO and HCl/Cl_2 from **2** exhibit 2, 3, 3 and 2 maxima, respectively, in different temperature ranges under helium atmosphere i.e. fragments are lost periodically in different temperature ranges.

Simultaneous EGA-MS of 2nd step of degradation of **2** under air atmosphere shows two maxima for the rate of evolution of fragments; one at lower temperature ~ 247 °C and other at higher temperature ~310 °C, however TG curve shows only one step enclosing both maxima of evolution during degradation unlike that under helium. Coincidence of the maxima for the fragments ions arising from the fragments CO and NH at lower temperature (247 °C) of 2nd step of degradation under air indicates that both CO and NH groups are degrading simultaneously at almost same temperature whereas under helium only NH group is undergoing degradation at 2nd step of decomposition. HCl / Cl_2 along with other ligand fragments are being lost at higher temperature (310 °C) in same way as in 3rd step of degradation of **2** under helium atmosphere. Similarly almost same gases are evolved under third step of degradation of **2** under air atmosphere as in 4th step of degradation under helium except CO in helium and CO_2 under air. Thermal degradation under air atmosphere is completed at ~ 600 °C for all the complexes whereas it is continued up to ~900 °C under helium.

Onset of thermal degradation of anhydrous complex **2** (2nd step of degradation) under helium as well as air atmospheres at lower temperature than that of **3** indicates that degradation of the ligand moiety is significantly influenced / accelerated by copper(II) ions bonded to it as compared to that of nickel(II) ions. Second step of thermal degradation of all other complexes under helium and air atmospheres except 2 under helium atmosphere is raised to such a high temperature that it is very close to 3rd step of degradation. Both steps of degradations result a combined TG curve, however, two separate maxima; one at slightly lower and other slightly higher temperature are obtained in simultaneous EGA-MS curves corresponding to 2nd and 3rd steps of degradation, respectively. Therefore, all the ligand dadb moiety directly bonded with copper(II) metal ions in the heterobimetallic complex **4**, would be expected to start degrading at almost same temperature as in case of **2**. Contrary to above, the onset of 2nd stage of degradation of **4** takes place at intermediate temperature between those of **2** and **3**, probably due to change of

electronic environment on Cu(II) atoms of **4** as a consequence of electronic communication between Cu(II) and Ni(II) ions bridged by π-conjugated dadb ligand [10,16]. Onset of degradation of **4** at higher temperature than that of **2** indicates that the ligand dadb moiety is less destabilized in **4** as compared to that of **2.** Similar correlation is found with DTA data of the complexes **2**, **3** and **4**.

Simultaneous EGA-MS scan of all the complexes under air as well as under helium atmospheres shows that NH, $HCN/(CN)_2$, CO/CO_2 and HCl/Cl_2 fragments are being lost periodically at different temperature ranges i.e. loss of fragments exhibits multiple maxima for the rate of evolution fragments. Due to presence of multiple maxima in EGA-MS scan of **2**, it is concluded that a fraction of evolved fragments recombine with complex residue to form a new complex residue stable at the temperature range for that step of degradation and rest fraction escapes. Newly formed complex residue starts to degrade on higher temperature and same cycle could be repeated / terminated depending upon fragment and nature of complex residue. In case of 3rd step of degradation of **2** under helium atmosphere, a fraction of fragment HCl/Cl_2 and CO molecules recombines with complex residue and liberates heat so this step becomes exothermic. Further, recombination process under 4th step of degradation of **2** is terminated so no heat is evolved, consequently this step of degradation becomes endothermic unlike 2nd step of degradation. Such correlation with other complexes **3** and **4** can't be explained due to partial overlap of 2nd and 3rd step of degradation of these complexes under helium and all the complexes under air atmospheres. Final residue under air and helium atmospheres corresponds to the metal oxide and metal alongwith some carbonaceous matter, respectively.

Acknowledgements

Authors are thankful to Head, Department of Chemistry for providing laboratory facilities, recording of IR, and DSC curves. Financial assistant from UGC New Delhi in form of a project is gratefully acknowledged. Prof. R. K. Mandal, department of Metallurgy, IT, BHU is gratefully acknowledged for recording PXRD of metal complexes. Thanks are also due to SAIF, Cochin for providing TG, DTG and DTA curves under air atmosphere at PED thermal analyzer. Imre M. Szilágyi thanks for a János Bolyai Research Fellowship of the Hungarian Academy of Sciences.

Supplementary Information

Table S1 containing IR spectral data of complexes, position of selected intense peaks in powder XRD spectra of the complexes in table S2, and Table S3 a-e giving thermal analysis data of the complexes **2**, **3** and **4** under air as well as under helium atmospheres, Fig. S1 showing TG and DTA curves of **2**, **3** and **4** recorded on TA thermal analyzer with heating rate 15 °C/min under air atmosphere, Fig. S2 a-c presenting EGA-MS plot of **2**, **3** and **4** under air atmosphere on the heating rate 10 °C/min, Fig. S3 a-c presenting EGA-MS plot of **2**, **3** and **4** under helium atmosphere on the heating rate 15 °C/min, Fig. S 4 a-c presenting EGA-MS plot of **2**, **3** and **4** under air atmosphere on the heating rate 15 °C/min, Fig. S5 a-c presenting TG curves of **2**, **3** and **4** under helium as well as under air atmospheres on the heating rate 15 °C/min and 10 °C/min and Fig. S 6 presenting TG curves of **2**, **3** and **4** under air at the heating rate 10 °C/min and helium atmospheres at the heating rate 10 °C/min are given in supplementary information file.

References

1. Condorelli GG, Malandrino G, Fragala I, Metal-Organic Chemical Vapor Deposition of Copper and Copper(I) Oxide: Kinetics and Reaction Mechanisms in the Presence of Oxygen. Chem Mater. 1995;7(11):2096–2103.
2. Poizot P, Laruelle S, Grugeon S, Dupont L, Taracon JM. Nano-sized transition-metal oxides as negative-electrode materials for lithium-ion batteries. Nature. 2000;407:496–499.
3. Mac Donald AH. A technique for injecting electrons into the surface layers of materials has now been applied to the most mysterious of superconducting compounds — the copper oxides. Nature. 2001;414:409–410.
4. Kumar RV, Diamant Y, Gedanken A. Sonochemical Synthesis and Characterization of Nanometer-Size Transition Metal Oxides from Metal Acetates. Chem Mater. 2000;12(8):2301–2305.
5. Gao XP, Bao JL, Pan GL, Zhu HY, Huang PX, Wu F, Song DY. Preparation and Electrochemical Performance of Polycrystalline and Single Crystalline CuO Nanorods as Anode Materials for Li Ion Battery. J Phys Chem. B. 2004;108:5547–5551.
6. Maruyama T. Copper oxide thin films prepared by chemical vapor deposition from copper dipivaloylmethanate. Sol Energy Mater Sol Cells. 1998;56:85–92.

7. Ramirez-Ortiz J, Ogura T, Medina – Valtierra J, Acosta-Ortiz SE, Bosch P, De Los Reyes JA, Lara VH. A catalytic application of Cu_2O and CuO films deposited over fiberglass[J]. Appl Surf Sci. 2001;174:177–184.

8. Allmendinger T. Synthesis and characterization of metal containing polychloranilamides; Macromol Chem Phys. 1997;198:4019–4034.

9. Prasad RL, Kushwaha Anita, Singh Deepshikha. Synthesis, characterization and thermal degradation of 1-D coordination polymers of the type $CuxZn_{1-x}$(dadb).yH_2O(dadb=2,5-diamino-3,6-dichloro-1,4-benzoquinone; and x=1.0, 0.5, 0.0625 and 0). Therrmochimica Acta. 2010;511(1-2):17 –26.

10. Prasad RL, Kushwaha A, Suchita, Kumar M, Yadav RA, Infrared and ab initio studies of conducting molecules: 2,5-diamino-3,6-dichloro-1,4-benzoquinone. Spectrochim. Acta. 2008;A 69: 304 – 311.

11. Creutz C, Taube H. Binuclear complexes of ruthenium ammines. J Am Chem Soc. 1973; 95:1086–1094.

12. Cao M, Hu C, Wang Y, Guo Y, Guoa C, Wanga E, A controllable synthetic route to Cu, Cu_2O, and CuO nanotubes and nanorods. Chem.Comm. (2003) 1884–1885.

13. Furmiss BS, Hannaford AJ, Rogers B, Smith PWG, Tatchell AR. Vogel's Text Book of Practical Organic Chemistry; ELBS 4th ed., 1978.

14. Fieser LF, Martin EL. A comparison of heterocyclic systems with benzene.VII. Isologs of anthraquinone containing one and two triazole rings. J Am Chem Soc. 1935;57:1844.

15. Matsunaga Y, McDowell CA. The electron spins resonance absorption spectra of semiquinone ions part II. The hyperfine splitting due to amino groups. Can J Chem. 1960;38:1167–1171.

16. Prasad RL, Kushwaha A, Shrivastava ON, Synthesis, characterization and solid state electrical properties of 1-D coordination polymer of the type $[Cu_xNi_{1-x}(dadb)_yH2O]_n$. J Solid state Chem. 2012;196:471-481.

17. D'Souza L, Devi P, Shridhar MPD, Naik CG. Use of fourier transform infrared (FTIR) spectroscopy to study cadmium-induced changes in *Padina Tetrastromatica* (Hauck). Anal Chem Insights. 2008;3:135–143.

18. Kuramshin AI, Kuramshina EA, Cherkasov RA. Synthesis of mesityl oxide p-complexes with metals of chromium subgroup and with iron. Theoretical and experimental investigation of the ligand dissociation energy. Russ. J. Org. Chem. 2005;41:649-655.

19. Kawata S, Kitagawa S, Furuchi I, Kudo C, Kamesaki H, Kondo M, Katada M, Munakata M. Synthesis, structure, and magnetic properties of crystalline coordination polymers of copper(II),{[Cu(CA)(H_2O)$_2$(H_2O)}$_n$ and [Cu(CA)(MeOH)$_{2n}$ (H_2CA; chloranilic acid)]. Mol Cryst Liq Cryst. 1995;274:179–185.

20. Azaroff LV, Buerger MJ. The Powder Method in X-ray Crystallography. New York: McGraw-Hill; 1958;119.

21. Sallam SA. Binuclear copper(II), nickel(II) and cobalt(II) complexes with N_2O_2 chromophores of glycylcine Schiff – bases of acetylacetone, benzoylacetone and thenoyltrifluroacetone. Trans Met Chem. 2006;31:46–55.

22. Madarász J, Szilágyi IM, Hange F, Pokol G. Comparative evolved gas analyses (TG-FTIR, TG/DTA-MS) and solid state (FTIR, XRD) studies on thermal decomposition of ammonium paratungstate tetrahydrate (APT) in air. J. Anal. Appl. Pyrolysis 2004; 72 : 197–201.

23. Szilagyi IM, Madarasz, J, Pokol G, Kiraly P, Tarkanyi G, Saukko S, Mizsei J, Toth AL, Szabo A, Varga-JosepovitsO K. Stability and Controlled Composition of Hexagonal WO3. *Chem. Mater.* **2008,** *20,* 4116–4125.

24. Akama Y. Thermal decomposition of copper complexes of 1–phenyl–3–methyl-4–acyl–5–pyrazolone in air atmosphere. J Thermal Analysis. 1995;45:1501–1506.

25. Abdalla EM, Said AA. Thermal studies on cobalt(II), nickel(II) and copper(II) ternary complexes of N-(2-acetamido)iminodiacetic acid and imidazoles. Thermochim. Acta. 2003;405:269–277.

26. Verma R K, Verma L, Chandra M, Bhushan A. Non-isothermal dehydration and decomposition of dl-lactates of transition metals and alkaline earth metals. A comparative study. J. Therm Anal and Calorim. 2005;80:351–354.

27. Yang Z, Xu J, Zhang W, Liu A, Tang S. Controlled synthesis of CuO nanostructures by a simple solution route. J. Solid State Chem. 2007;180:1390–1396.

28. Roman P, C. Guzmam-Miralles, A. Luque, Seco ML. Studies on the thermal decomposition of dipotassium trans-diaquabis(oxalato-O,O')nickelate(II) tetrahydrate. Thermochim. Acta 1995;257:67-73.

29. Lay E, Song Y-H, Chiu Y-C, Lin Y-M, Chi Y. New CVD precursors capable of depositing copper metal under mixed O2/Ar atmosphere, Inorg. Chem. 2005;44:7226 −7233.

30. Akanni MS, Ajayi OB, Lanbi JN. Pyrolytic decomposition of some even chain length copper(II) carboxylates. J Therm Ana. 1986;31:131–143.

31. Krunks M, Leskela T, Mannonen R, Niinisto L. Thermal decomposition of copper(I) thiocarbamide chloride hemihydrates. J Therm Anal. Calorim. 1998;53:541–544.

FIGURES

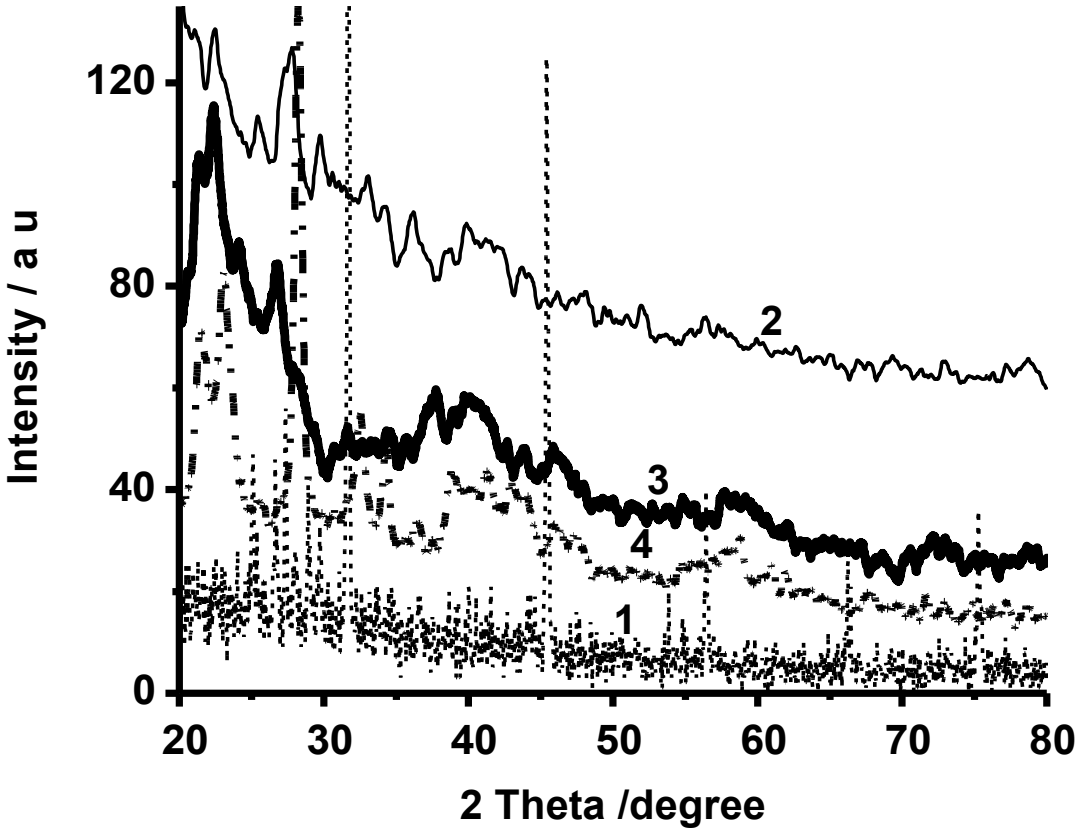

Fig. 1 Powder XRD pattern of **1** – **4**.

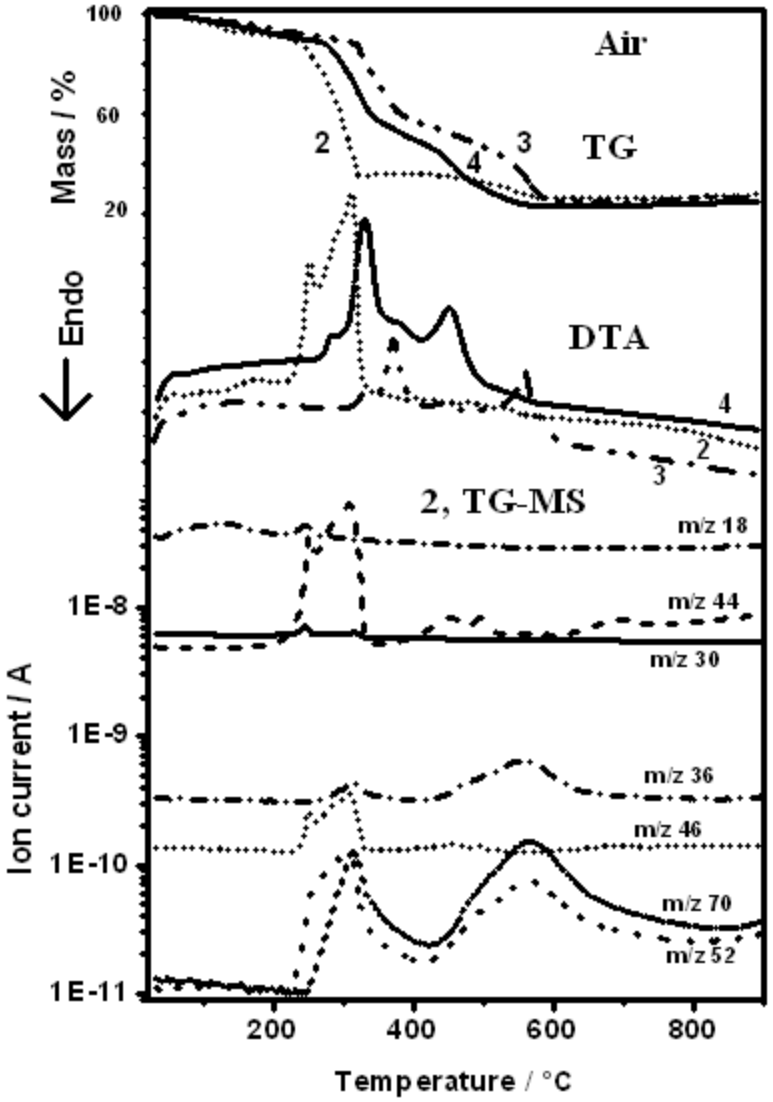

Fig. 2 TG, and DTA curves of **2**, **3** and **4** and simultaneous EGA-MS of selected ion evolved from **2** under air atmosphere with heating rate 10 °C/min.

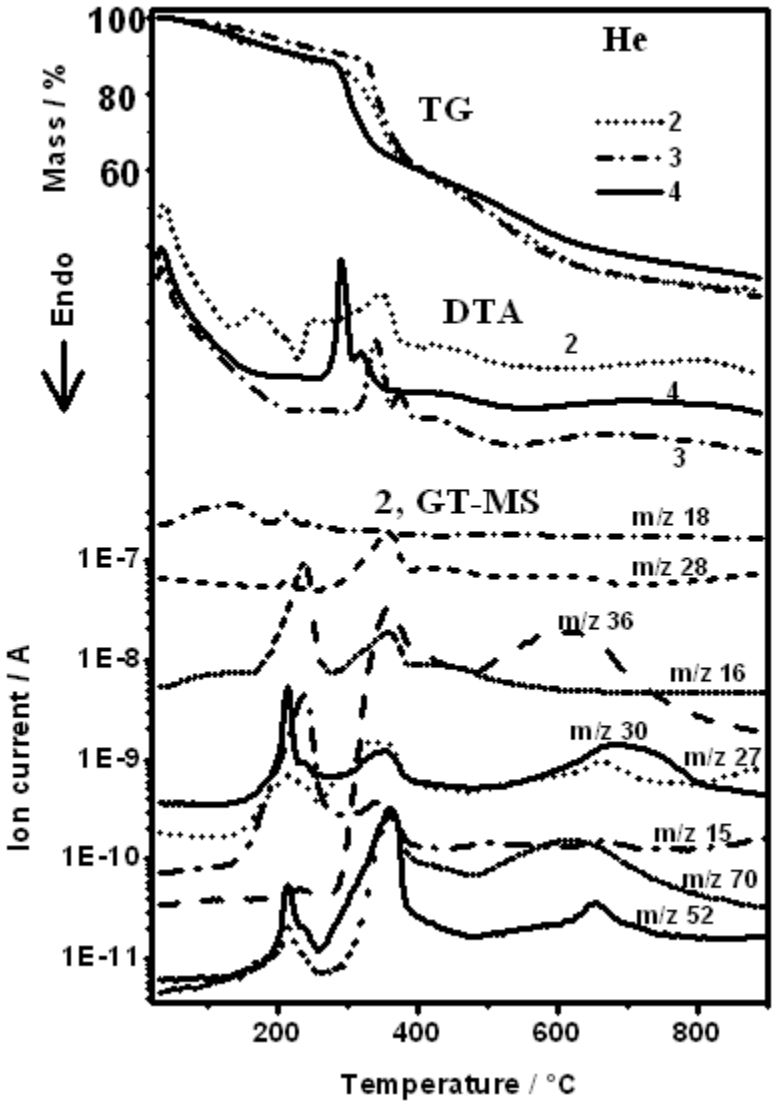

Fig. 3 TG, and DTA curves of **2**, **3** and **4** and simultaneous EGA-MS of selected ion evolved from **2** under helium atmosphere with heating rate 15 °C/min.

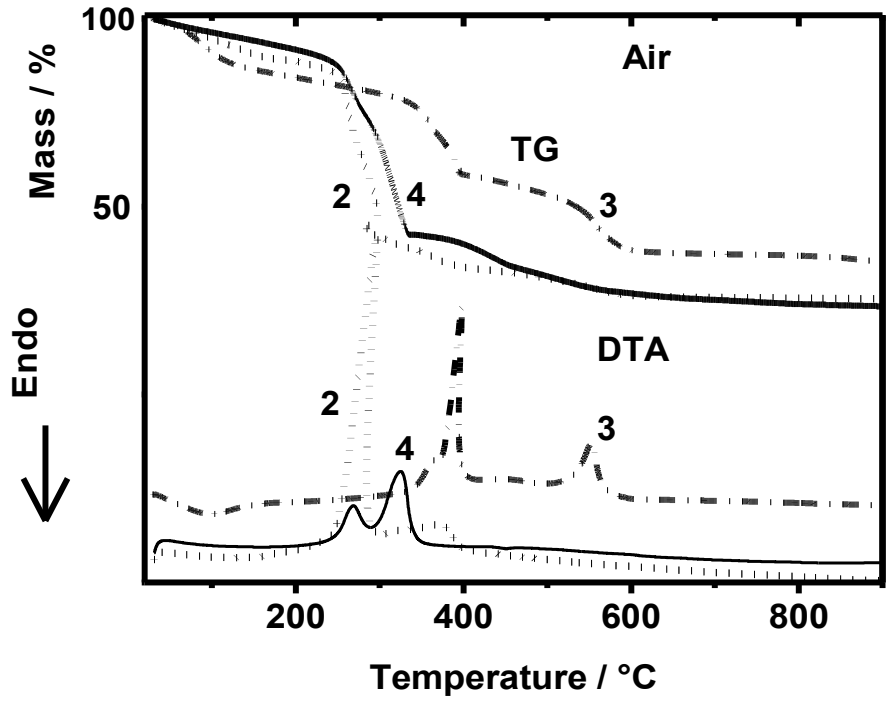

Fig. 4 TG and DTA curves of **2**, **3** and **4** under air atmosphere with heating rate 15 °C/min recorded on Perkin Elmer Diamond (PED) thermal analyzer .

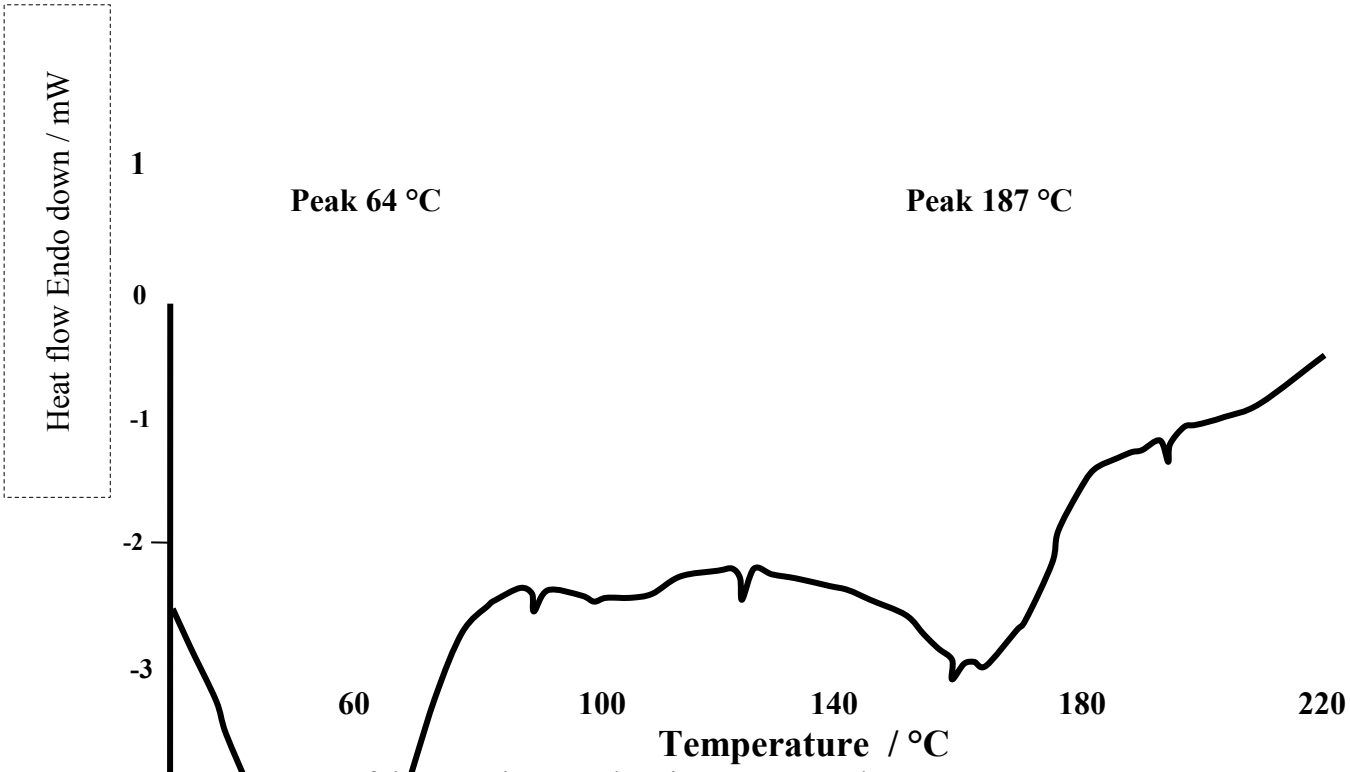

Fig. 5 DSC curve of the complex **3** under nitrogen atmosphere**.**

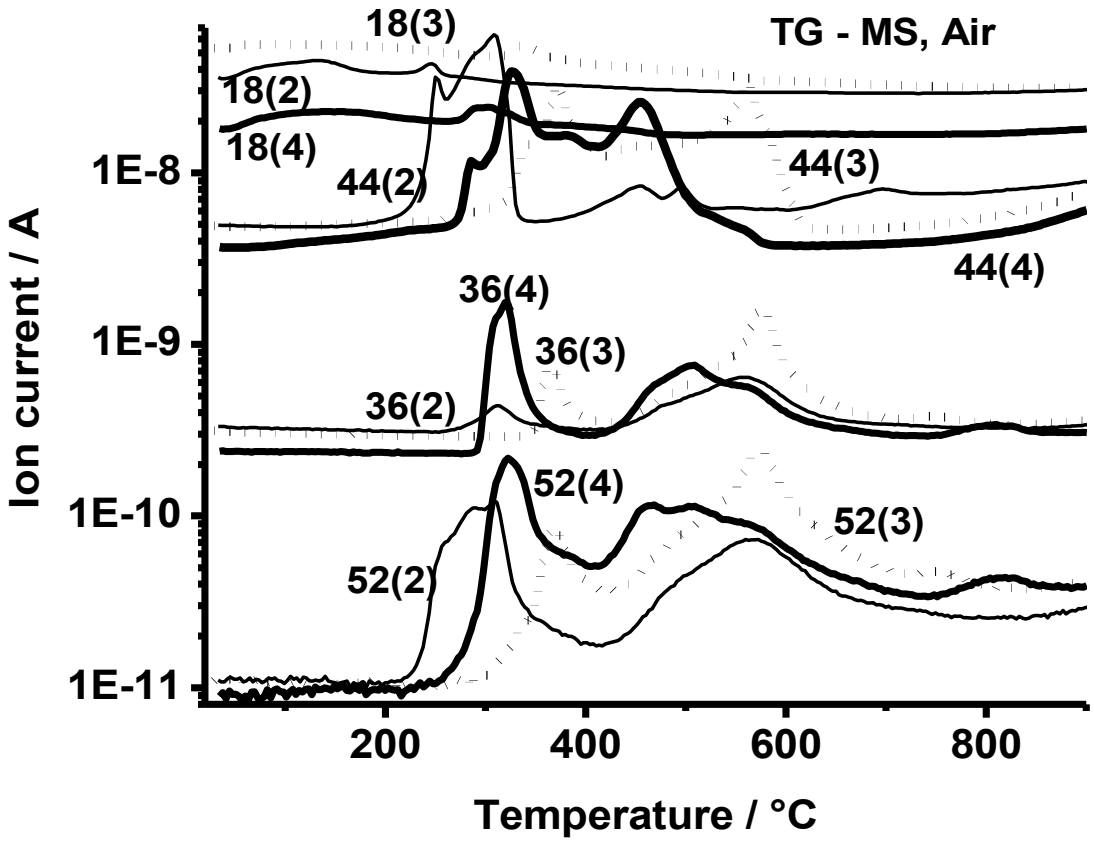

Fig. 6 Selected ions EGA-MS scan for the **2**, **3** and **4** at heating rate 10 °C /min under air atmosphere.

Supplementary Information

Solid state thermal degradation behaviour of heterobimetallic 1-D coordination polymers bridged by conjugated ligand

Ram Lakhan Prasad[*1], Anita Kushwaha[1], Imre Miklós Szilágyi[2] and László Kótai[3]

[1] Department of Chemistry, Faculty of Science, BHU, Varanasi-221005, India.
[2] Research Group of Technical Analytical Chemistry of the Hungarian Academy of Sciences, Department of Inorganic and Analytical Chemistry, Budapest University of Technology and Economics, H–1111 Budapest, Szt. Gellért tér 4. Hungary.
[3] Research Centre for Natural Sciences, Hungarian Academy of Sciences, Pusztaszeri u. 59-67, Budapest, Hungary, H-1025.

Table S 1 Important IR spectral bands /cm^{-1} and their assignments

Compounds	ν (OH)	ν (NH_2)	ν (C = O)	ν (C = C) ring	β NH_2
1	-	3308s 3376 s	1667 ms	1616 s	1580 vs
2	3470 bs	3282 m	1653 ms	1542 sh	1494 vs
4	3446 bs	3324 ms	1610 ms	1519 vs	1519 vs
5	3423 bs	3337 ms	1611ms	1518 vs	1518 vs
3	3404 bs	3317 ms	1619 ms	1515 vs	1515 vs

Table S 2 Position of selected intense peaks in Powder XRD spectra of complexes

Complex	**2**		**4**		**3**	
Peak	Angle /2θ	d-space / Å	Angle /2θ	d-space /Å	Angle / 2θ	d-space /Å
1	–	–	21.43	4.14	21.42	–
2	22.34	3.98	23.05	3.86	22.48	3.95
3	27.08 27.68 27.85	3.29 3.22 3.20	28.18 s	3.16	26.72	3.33
4	33.08	–	32.59	2.75	–	–
5	34.32	–	34.37	2.61	–	–
6	36.04	2.49	38.58	2.33	37.84	2.38

Table S 3 (a) Thermal analysis data for **2** under air atmosphere

Recorded on PED (@ 15 °C/ min) Cudadb·2H_2O: M.W. 304.54				Recorded on TA Instrument (@ 15 °C/ min) Cudadb·1.2H_2O: M.W. 290.14					Recorded on TA Instrument (@ 10 °C/ min) Cudadb·1.2H_2O: M.W. 290.14				
Temp. range / °C	Mass loss / % (Residue)	DTG peak / °C	DTA Peak / °C	**Temp. range / °C**	Mass loss / % (Residue	DTG peak / °C	DTA Peak / °C	MS signal corresponding to the composition	**Temp. range / °C**	Mass loss / % (Residue	DTG peak / °C	DTA Peak / °C	MS signal corresponding to the composition
RT – 200	11.0(11.82) (89)	150	45 exo 150endo	**RT -200**	7.5 (92.5)	140		H_3O (19), H_2O (18), OH (17)	**RT-200**	7.4 (92.6)	76 127	76 endo 131 endo	H_3O (19), H_2O (18), OH (17)
200 – 297.5	41/52 (48)	220 w 245 sh 263	297 exo	**200-257**	6.1/ 13.6 (86.4)	240	247 exo	H_3O, NH_4/ H_2O, NH_3/OH, NH (15), NO (30), CO_2/ N_2O (44), NO_2 (46), C(12), $(CN)_2$ (52, 26), C_2OCl (75),	**200 - 325**	57.25/ 64.65 (35.35)	246 310	250 exo 311 exo	NH_3/ H_2O, NH_3/ OH, NO (30), CO_2/ N_2O (44), NO_2 (46), C(12), $(CN)_2$ (52), HCl (36, 38), Cl_2 (70,72, 35, 37), small amount of C_3Cl (71), C_2OCl (75), C_3OCl (87) CuCl (98), $CuCl_2$ (133)
297 –284 - 330	8.7/60.7 (39.3)	290 sh 313		**257-310**	39.4 /53 (47)	276	308 exo	NH_4/ H_2O, NH_3/OH, CO_2/ N_2O, NO_2, HCl (36, 38), Cl_2 (70,72, 35, 37), C, C_4 (48), $(CN)_2$, C_3Cl (71), C_2OCl, C_3OCl (87), CuCl (98), $CuCl_2$ (133)					
330 -420	5.8/ 66.5 // 55.5 (33.5)	366	372 exo	**310-304-337**	9.5/62.5 //55 (37.5)	325 sh	325 exo	CO_2/ N_2O, NO, C, C_4, $(CN)_2$, HCl, Cl_2, C_3Cl (71), C_2OCl, C_3OCl , CuCl , $CuCl_2$					
				337 -370 -410	0/62.5 (37.5)	-	-	C_4, and traces of HCl, CO_2, Cl_2, C_3Cl , C_2OCl, C_3OCl	**325-430**	-0.4/ 64.25 (35.75)	-	398 exo	Traces of HCl, Cl_2, CO_2, and $(CN)_2$,
420 - 600	7 / 73.5 (26.5) calc. for CuO (26.12)	560		**410-820**	26.9/ 89.4 (10. 6)	655		C_4, HCl, Cl_2, $(CN)_2$ and traces of CO_2,C_3Cl, C_2OCl.	**430-600**	10.25/74 (26)	462 540	478 exo	HCl, Cl_2, $(CN)_2$, traces of CO_2, C_3Cl
			-		Calc. for CuO (27.4)				**600-900**	-1.6/ 72.4 (27.6) Calc. for CuO (27.4)	-	-	Traces of CO_2, HCl, Cl_2, $(CN)_2$, C_3Cl

PED = Perkin Elmer Diamond thermal analyzer,

Table S3 (b) Thermal analysis data for **3** under air atmosphere.

Recorded on PED (@ 15 °C/ min) Nidadb·4H_2O: M.W. 335.7				Recorded on TA Instrument (@ 15 °C/ min) Nidadb·1.5H_2O: M.W. 290.7					Recorded on TA Instrument (@ 10 °C/ min) Nidadb·1.5H_2O: M.W. 290.7				
Temp. range / °C	Mass loss / % (Residue	DTG peak / °C	DTA Peak / °C	**Temp. range / °C**	Mass loss / % (Residue	DTG peak / °C	DTA Peak / °C	MS signal corresponding to the composition	**Temp. range / °C**	Mass loss / % (Residue	DTG peak / °C	DTA Peak / °C	MS signal corresponding to the composition
RT – 300	20.5(21.44) (79.5)	80	35 exo 100 Endo	**RT-300**	9.3/(9.28) (90.7)	80 215	90 endo 237 endo	H_2O (18), OH (17)	**RT-280**	9/(9.28) (91)	60 205	70 endo 220 endo	H_2O (18), OH (17)
300 – 420	21.0/41.5 (58.5)	358 384	365 exo 398 exo	**300 - 460**	40.7/50 (50)	330 370 412	340exo 380exo 413exo	NH_4/ H_2O, NH_3/OH, CO_2/ N_2O (44), NO_2 (46), C(12), C_4(48), HCl (36, 38), Cl_2 (70,35, 37, 72), **$(CN)_2$ (52)**, C_3Cl (71), C_2OCl (75), C_2OCl (75)	**280 - 410**	35/ 44 (56)	323 345 366	335 exo 370 exo	NH_4/ H_2O, NH_3 / OH(17), CO_2/ N_2O (44), NO_2 (46), C(12), **$(CN)_2$ (52)**, HCl (36, 38), Cl_2 (70, 72, 35, 37) C_3Cl (71), C_2OCl (75),
420 – 620	20.5/62.0 (38)	550 575 sh	450 exo 553 exo	**475-900**	30.3/80.3 19.7 Calc. for NiO (25.7)	570 590sh	570 exo 602 exo	NH, NO (30), CO_2/ N_2O, NO_2, HCl (36, 38), Cl_2(70,72, 35, 37), C, C_4 **$(CN)_2$**, C_3Cl (71), C_2OCl (75), C_3OCl (87)	**410-670**	31.5/ 75.5 (24.5)	555	440 exo 556 exo	CO_2/ N_2O (44), NO (30), NO_2 (46), C(12), **$(CN)_2$ (52)**, HCl (36, 38), Cl_2 (70, 72, 35, 37), C_3Cl (71), C_2OCl (75), C_3OCl (87),
620 – 800 almost constant 800 – 950	38.0/(37.75) gradual loss 3.0 (35) Calc. for NiO (22.25)	900							**670-900**	26.8 Calc. for NiO (25.7)	-		Traces of HCl, CO_2, Cl_2, **$(CN)_2$**,

Table S3 (c) Thermal analysis data for **4** under air atmosphere.

Recorded on PED (@ 15 °C/ min) $Cu_{0.5}Ni_{0.5}$dadb·1.75H_2O: M.W. 297.62				Recorded on TA Instrument (@ 15 °C/ min) $Cu_{0.5}Ni_{0.5}$dadb·1.75H_2O: M.W. 297.62					Recorded on TA Instrument (@ 10 °C/ min) $Cu_{0.5}Ni_{0.5}$dadb·1.75H_2O: M.W. 297.62				
Temp. range / °C	Mass loss / % (Residue)	DTG peak / °C	DTA Peak / °C	**Temp. range / °C**	Mass loss / % (Residue)	DTG peak / °C	DTA Peak / °C	MS signal corresponding to the composition	**Temp. range / °C**	Mass loss / % (Residue)	DTG peak / °C	DTA Peak / °C	MS signal corresponding to the composition
RT – 230	10.3/(10.58) (89.7)	–	38 exo 120-200 br.endo	**RT-250**	10.4/(10.58) (89.6)	98 173	136 endo	**H_3O (19), H_2O (18), OH (17),** NH (15), CN (26)	**RT-250**	10/(10.58) (90)	146	60 exo 85 endo	H_3O (19), H_2O (18), OH (17),
230 – 335	47.7/ 58 (42)	264 312	268 exo 326 exo (290-360)	**250-380**	38.3/48.7 (51.3)	300 321	292 exo 341 exo	H_3O, NH_4/ H_2O, NH_3/OH, NO (30), CO_2/ N_2O (44), NO_2 (46), C(12), C_2(24), C_4(48), HCl (36, 38), Cl_2 (70,35, 37, 72), **$(CN)_2$ (52)**, C_3Cl (71), C_2OCl (75), C_3OCl (87), CuCl (98), $CuCl_2$(133)	**245-360**	34/44 (56)	280 sh 318	286 exo 330 exo	H_3O, NH_4/ H_2O, NH_3 / OH(17), **NO (30),** CO_2/ N_2O (44), NO_2 (46), C(12), **$(CN)_2$ (52)**, HCl (36, 38), Cl_2 (70, 72, 35, 37) C_3Cl (71), C_2OCl (75), C_3OCl (87), CuCl (98), $CuCl_2$(133)
335 – 460	8.0/66 (34)	432	450 endo	**380-500**	20/68.7 (31.3)	460	459	NH, NO (30), CO_2/ N_2O, NO_2, HCl (36, 38), Cl_2(70,72, 35, 37), C, **$(CN)_2$**, C_3Cl (71), C_2OCl (75), C_3OCl (87), CuCl (98), $CuCl_2$(133)	**360 - 410**	8/52 (48)	380	381 exo	CO_2/ N_2O (44), NO (30), NO_2 (46), and traces of **$(CN)_2$ (52)**, HCl (36, 38), Cl_2 (70, 72, 35, 37), C_3Cl (71)
460 – 665	8.6 /74.6 (25.6)	515	Endothermic inclination	**500-900**	13/81.7 (18.3) Calc. for $Cu_{0.5}Ni_{0.5}O$ (25.53)	522 590		CO_2/ N_2O, NO_2, HCl (36, 38), Cl_2(70,72, 35, 37), **$(CN)_2$**, C_3Cl (71), C_2OCl (75), C_3OCl (87), CuCl (98), $CuCl_2$(133)	**410 - 600**	25/77 (23)	450 540 sh	450 exo	CO_2/ N_2O (44), NO (30), NO_2 (46), **$(CN)_2$ (52)**, HCl (36, 38), Cl_2 (70, 72, 35, 37), C_3Cl (71), C_2OCl (75), C_3OCl (87), CuCl (98), $CuCl_2$(133)
>665	Residue 25.4 Calc. for $Cu_{0.5}Ni_{0.5}O$ (25.91)								**600 -900**	(24.6) Calc. for $Cu_{0.5}Ni_{0.5}O$ (25.53)			Traces of HCl, CO_2, Cl_2, **$(CN)_2$**,

Table S 3 (d) Thermal analysis data for **2** and **3** under helium atmosphere.

2 under Helium atmosphere (@ 15 °C/ min) Cudadb·1.2H_2O: M.W. 290.14					**3** under helium atmosphere (@ 15 °C/ min) Nidadb·1.5H_2O: M.W. 290.7				
Temp. range / °C	Mass loss / % (Residue)	DTG peak / °C	DTA Peak / °C	MS signal corresponding to the composition	**Temp. range / °C**	Mass loss / % (Residue)	DTG peak / °C	DTA Peak / °C	MS signal corresponding to the composition
RT - 170	7/(7.44) (93)	128	40 exo, 134 endo	H_3O (19), H_2O (18), OH (17)	**RT - 310**	9.5 /(9.29) (90.5)	75, 220	35 exo 70 endo 225 endo	H_3O (19), H_2O (18), OH (17)
170 - 260	6/13 (87)	203, 230	205 endo,230 endo	H_3O, NH_3/ H_2O, OH/ NH_3, NH_2(16), NH (15), N (14), NO (30), N_2O (44), NO_2 (46), CO (28), C(12), HCN (27), small amount of C_2 (24), C_4 (48), $(CN)_2$ (52, 26), C_3Cl (71), and traces of C_2OCl (75), C_3OCl (87) CuCl (98)	**310-440**	32/41.5 (58.5)	335	340 exo 375 exo	H_3O, NH_3/ H_2O, **NH_2(16), NH (15),** NO (30), N_2O (44), NO_2 (46), **CO (28)**, HCl (36, 38), Cl_2(70,72, 35, 37), C(12), C_2 (24), C_4 (48), **$(CN)_2$ (52, 26)**, C_3Cl (71), C_2OCl (75), C_3OCl (87)
260 - 480	36/49 (51)	350, 410 br w	350 exo 425 exo	CO, N, NH, NH_2, NO, N_2O, NO_2, C, HCN, HCl (36, 38), Cl_2(70,72, 35, 37), C_2 , small amount of C_4, **(CN)2,** C_3Cl (71), C_2OCl (75), Traces of C_3OCl, CuCl,					
480 - 760	20/69 (31)	530, 580	610 endo	HCl, HCN, Cl_2, NO, C, traces of C_4, $(CN)_2$, C_2OCl (75),	**440-700**	26.5/68 (32)	535	435 exo 540 endo 675 exo	CO, NH, NH_2, NO, N_2O, NO_2, HCl (36, 38), Cl_2 (70, 72, 35, 37), C, C_2 **$(CN)_2$**, C_3Cl (71), C_2OCl (75), C_3OCl (87),
760-900	3/72 (28) Calc. for metallic Cu (21.90)			C, C_4, and traces of CO, HCN, CN	**700-900**	5.5/73.5 (26.5) Calc. for metallic Ni (20.2)	-	-	CO, C, C_2, CN

Table S 3 (e) Thermal analysis data for **4** ($Cu_{0.5}Ni_{0.5}$dadb·1.75H_2O: M.W. 297.62) under helium atmosphere.

Temp. range / °C	Mass loss / % (Residue)	DTG peak / °C	DTA Peak / °C	MS signal corresponding to the composition
RT - 280	10.6/ (10.58) (89.4)	82, 165	35 exo, 176 and 250 endo	H_3O (19), H_2O (18), OH (17)
280-430	30.4/ 41 (59)	298	295 exo 320 exo	H_3O, NH_3/ H_2O, N (14), **NH_2(16), NH (15),** NO (30), N_2O (44), NO_2 (46), **CO (28**), HCl (36, 38), Cl_2(70,72, 35, 37), C(12), C_2 (24), C_4 (48), HCN (27), **$(CN)_2$ (52, 26)**, C_3Cl (71), C_2OCl (75), C_3OCl (87), CuCl (98).
430 - 750	23 / 64 (36)	550	553 exo	CO, N, NH, N_2O, NO_2, HCl (36, 38), Cl_2 (70, 72, 35, 37), C, C_4, HCN, **$(CN)_2$**, C_3Cl (71), C_2OCl (75),
750-900	4.6 / 68.6 (31.4) Calc. for mixed metal $Cu_{0.5}Ni_{0.5}$ (20.54)	-	-	CO, C, C_4, HCN, CN

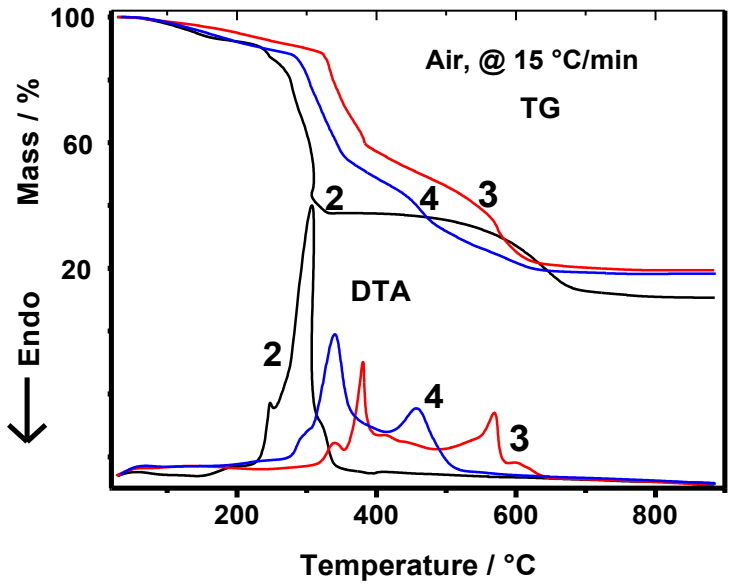

Fig. S1 TG and DTA curves of **2**, **3** and **4** recorded on TA thermal analyzer with heating rate 15 °C/min under air atmosphere.

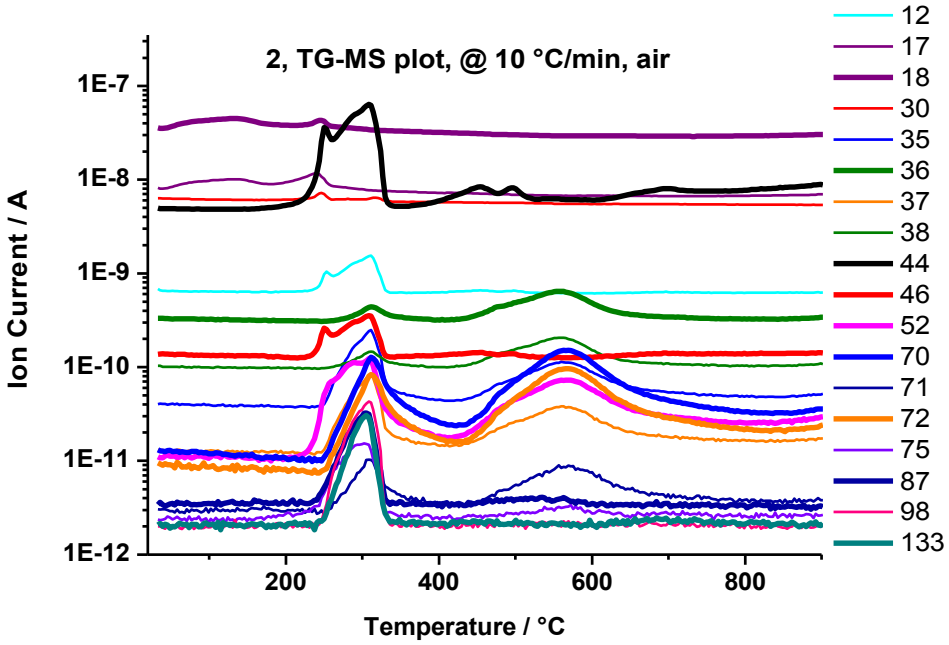

Fig. S2 (a) EGA-MS plot of **2** under air atmosphere with heating rate 10 °C/min.

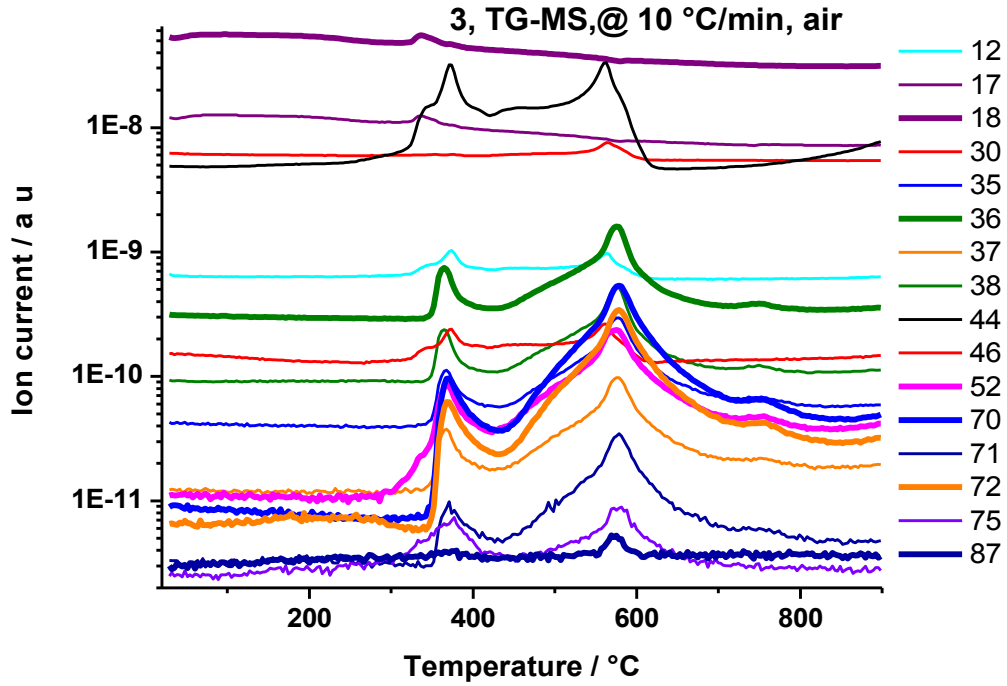

Fig. S2 (b) EGA-MS plot of **3** under air atmosphere with heating rate 10 °C/min

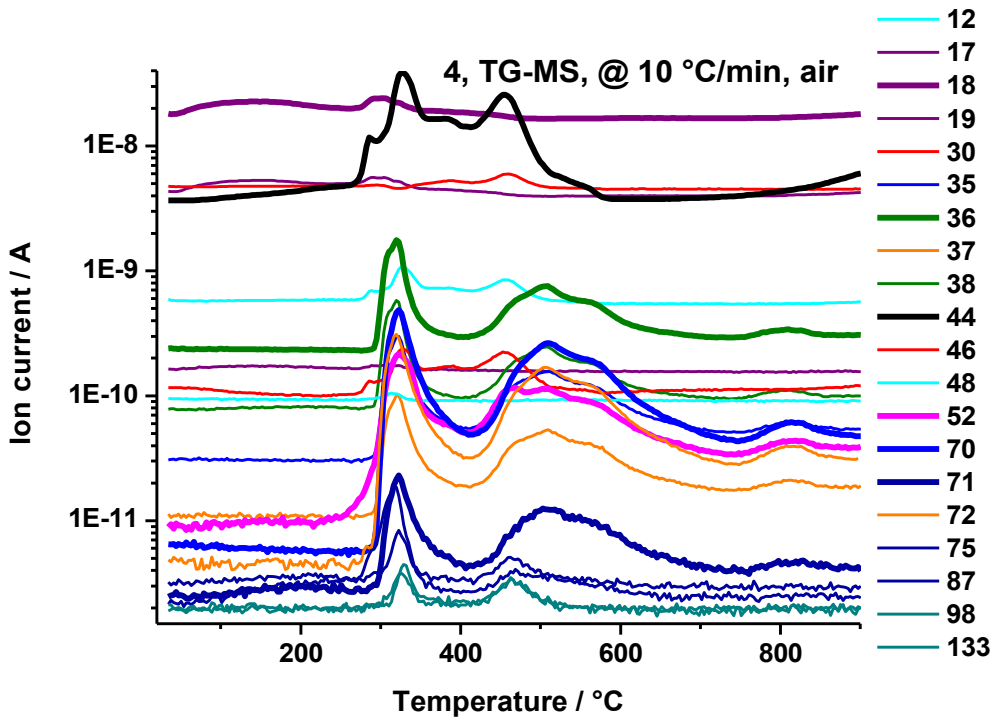

Fig. S2 (c) EGA-MS plot of **4** under air atmosphere with heating rate 10 °C/min.

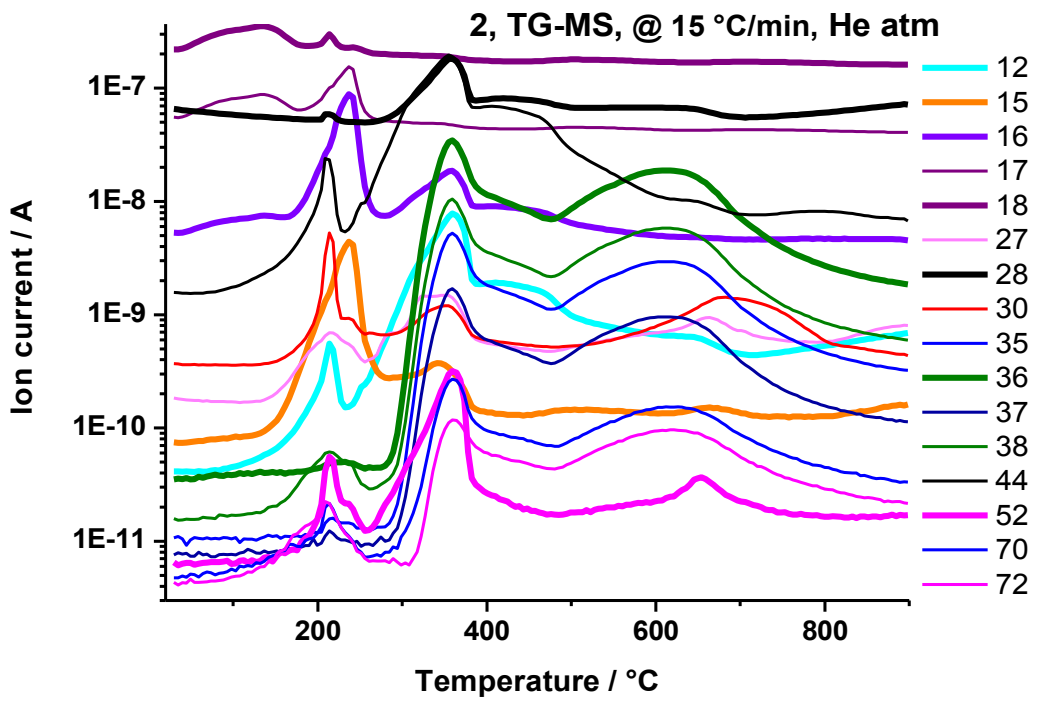

Fig. S3 (a1) EGA-MS plot of **2** under helium atmosphere with heating rate 15 °C/min.

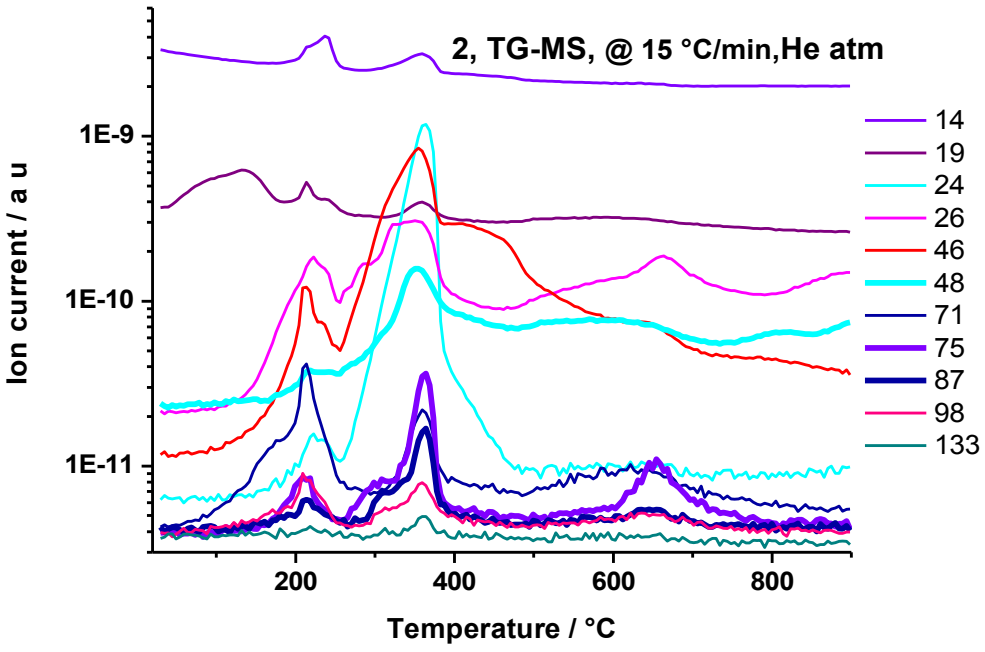

Fig. S3 (a2) EGA-MS plot of **2** under helium atmosphere with heating rate 15 °C/min.

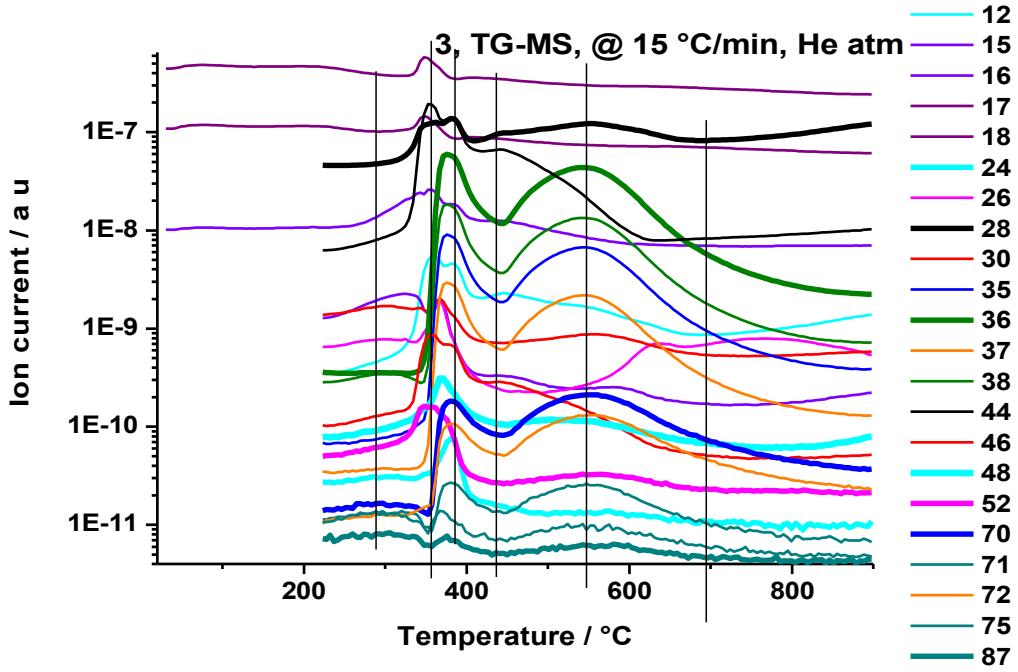

Fig. S3 (b) EGA-MS plot of **3** under helium atmosphere with heating rate 15 °C/min.

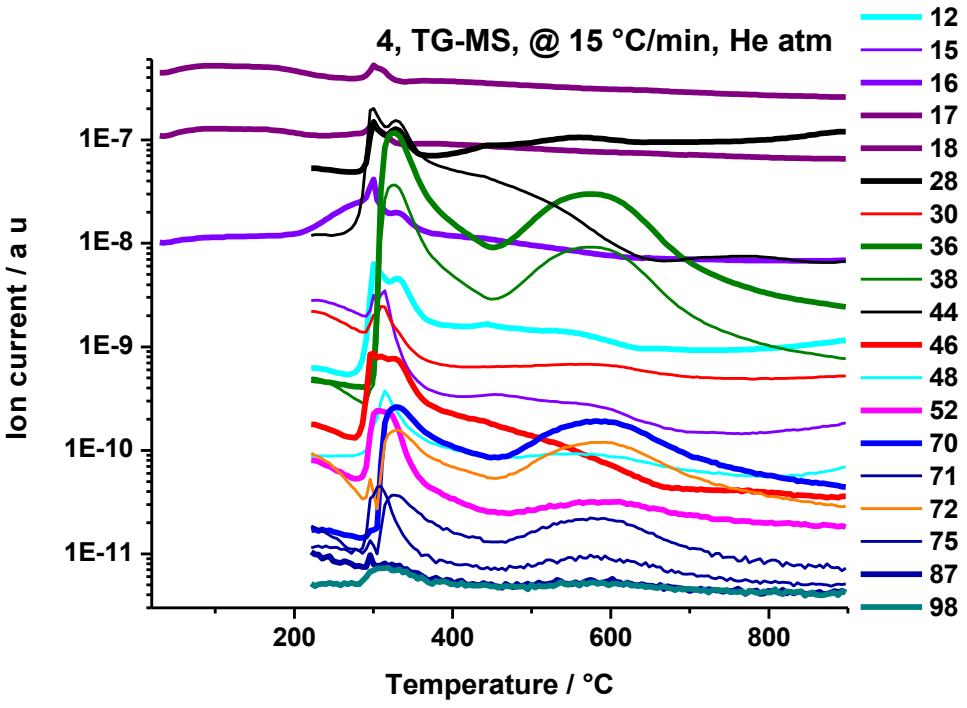

Fig. S3 (c) EGA-MS plot of **4** under helium atmosphere with heating rate 15 °C/min.

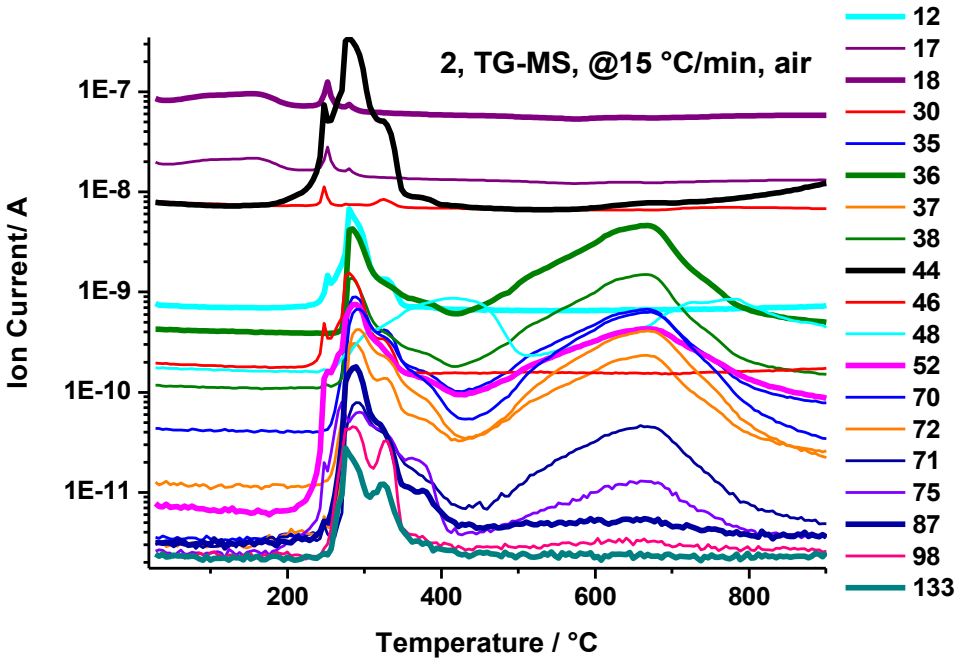

Fig. S4(a) EGA-MS plot of **2** under air atmosphere with heating rate 15 °C/min

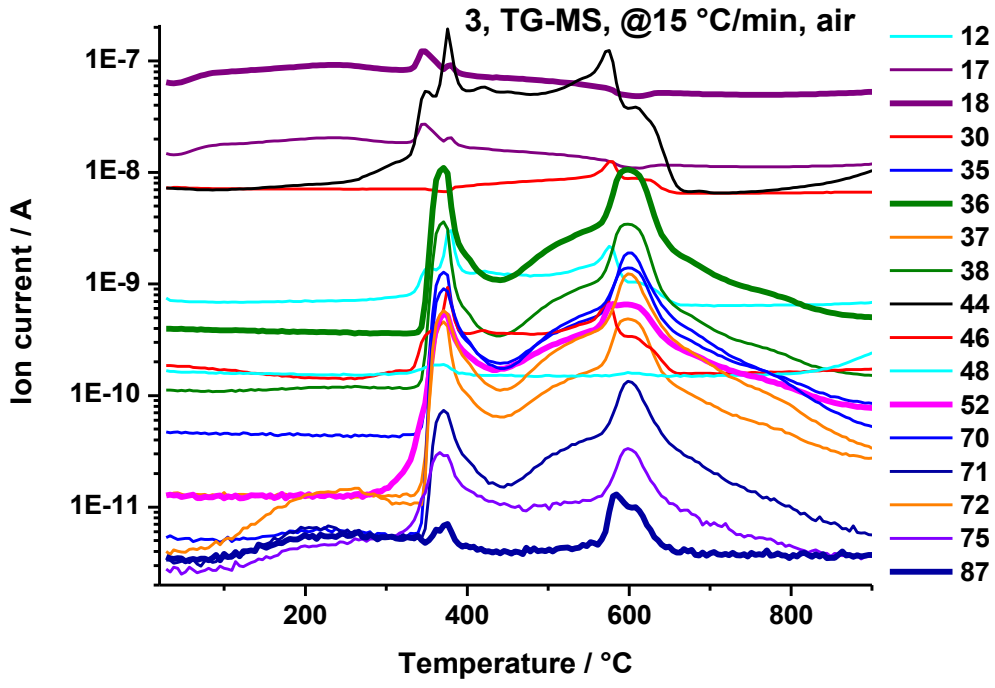

Fig. S4(b) EGA-MS plot of **3** under air atmosphere with heating rate 15 °C/min.

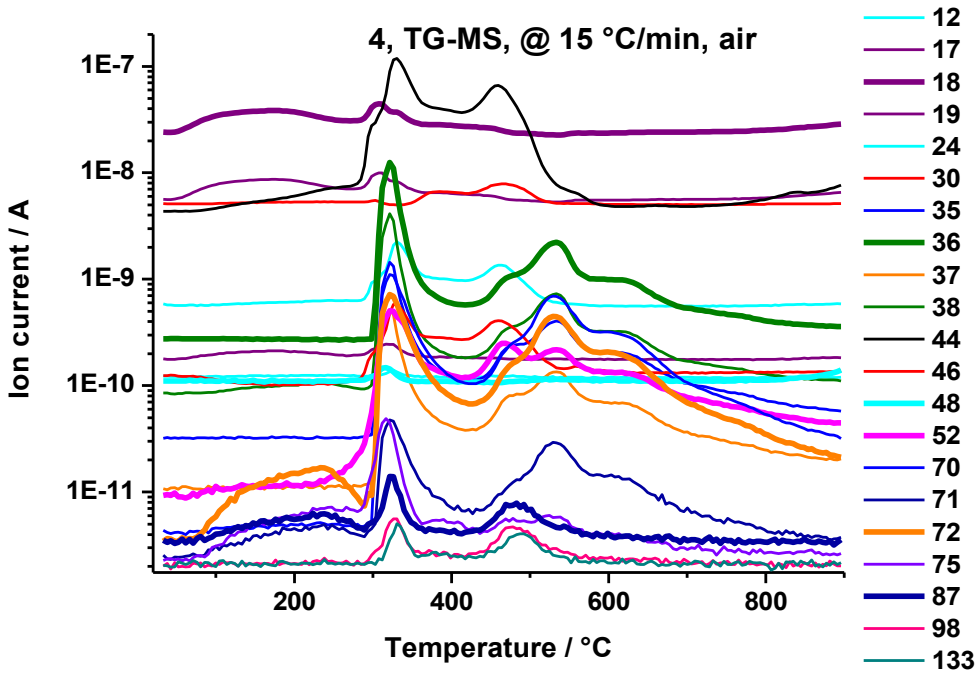

Fig. S4(c) EGA-MS plot of **4** under air atmosphere with heating rate 15 °C/min.

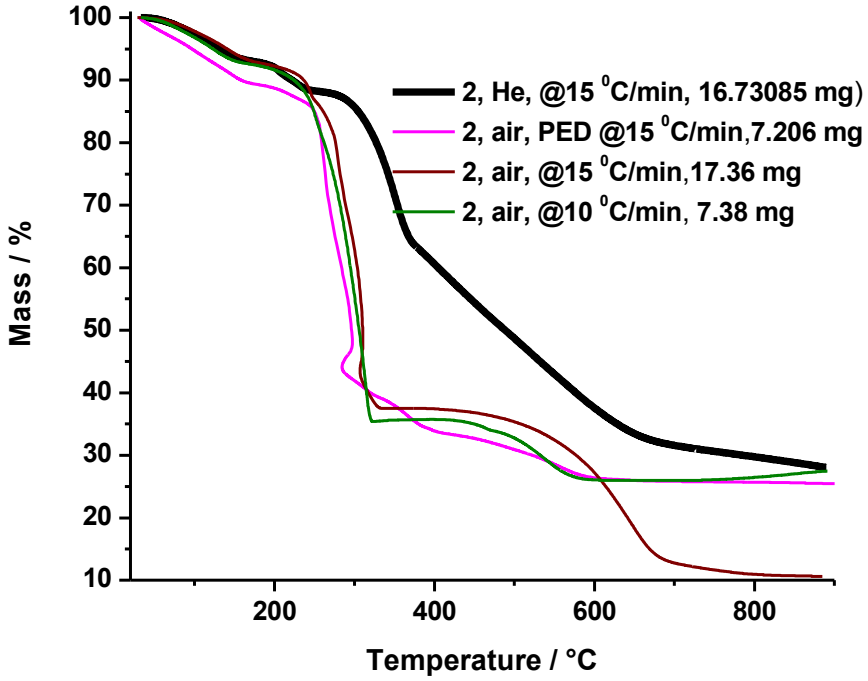

Fig. S5 (a) TG curves of 2, under air, and helium atmospheres .

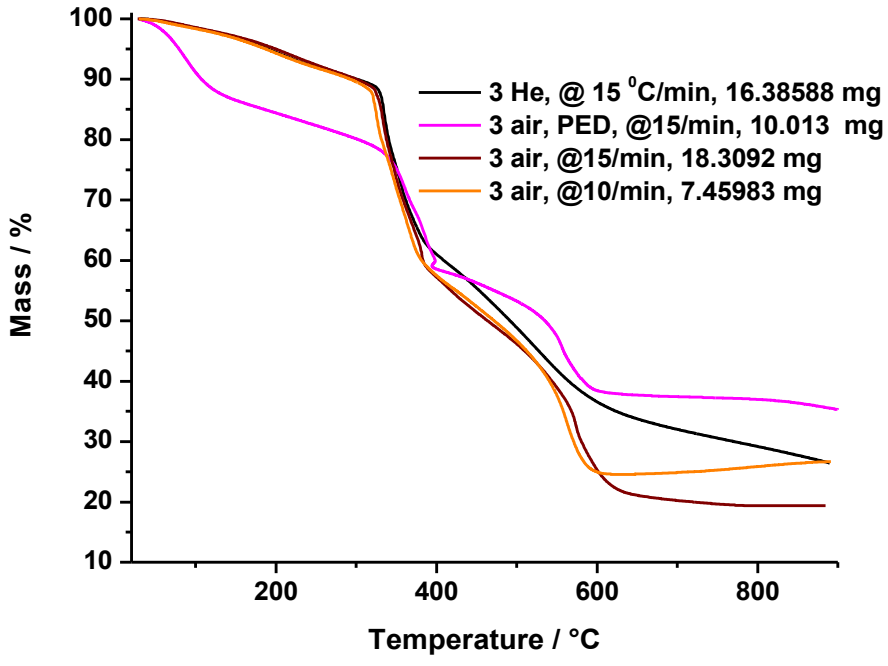

Fig. S5 (b) TG curves of 3, under air and helium atmospheres.

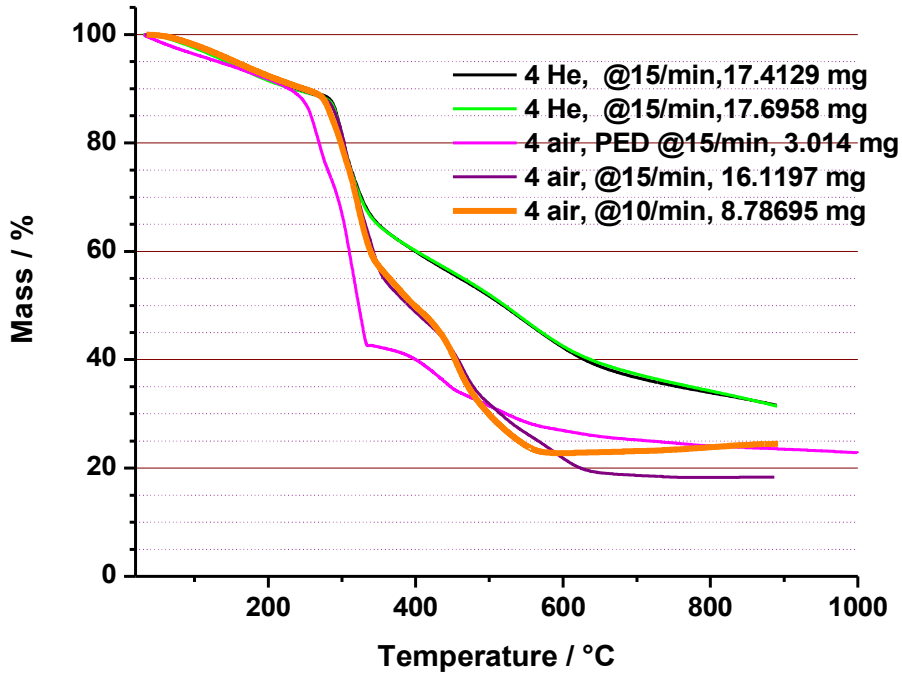

Fig. S 5 (c) TG curves of 4, under air and helium atmospheres

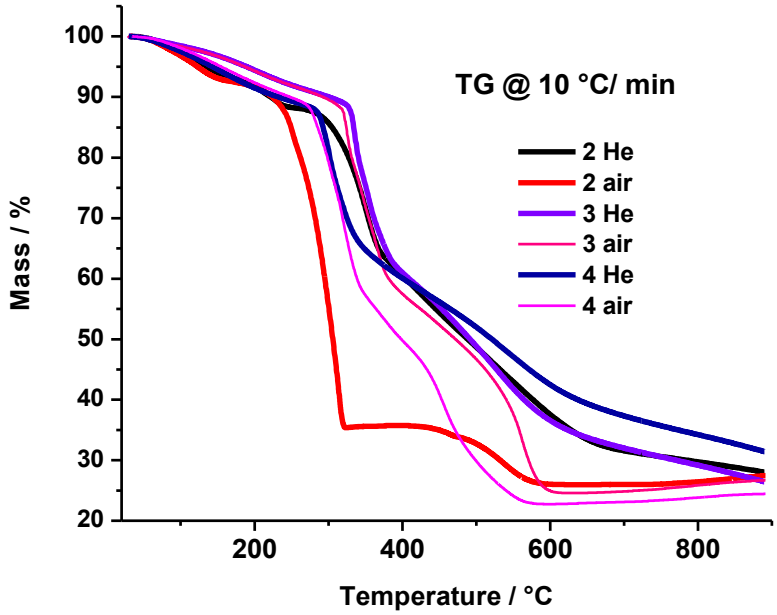

Fig. S 6 TG curves of **2**, **3** and **4** under air and helium atmospheres at the heating rate 10 °C/min.

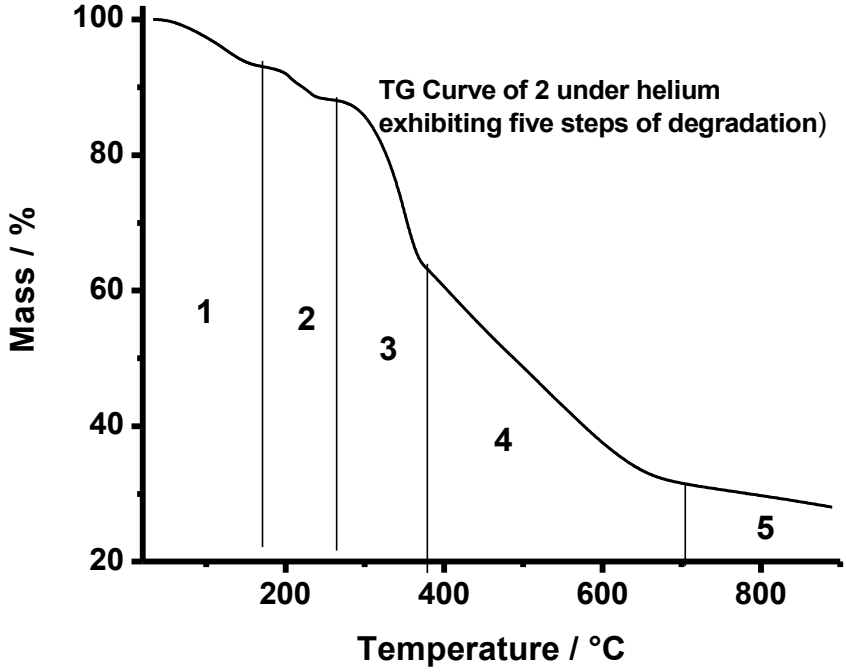

Fig. S 7 TG curves of **2** under helium atmosphere at the heating rate 15 °C/min showing five steps of thermal degradation.